Scientific and Technological Alliance for Guaranteeing the European Excellence in Concentrating Solar Thermal Energy

FP7 Grant Agreement number: **609837**
Start date of project: **01/02/2014**
Duration of project: **48 months**

STAGE-STE milestone 37

MS 37: Intermediate status of "Technology Roadmap to Solar Fuels" assessed

WP9 – Tasks 9.4	**Milestone 37 (MS37)**
Reached/Submitted:	**July 2016**
Work Package Leader:	**PSI**
Task leader:	**DLR**
Author(s):	**Anis Houaijia (DLR), Christian Sattler (DLR), Nathalie Monnerie (DLR), Manuel Romero (IMDEA), José González-Aguilar (IMDEA), Luca Turchetti (ENEA), Alberto Giaconia (ENEA), Domenico Mazzei (ENEA), Giampaolo Caputo (ENEA), Antonio Ienna (UNIPA), Benedetto Schiavo (UNIPA), Onofrio Scialdone (UNIPA), Alessandro Galia (UNIPA), Ludovic Charpentier (CNRS), Alfonso Vidal (CIEMAT), Aleix Jové Llovera (ABENGOA)**
Revised by:	**All Partners**
Document version:	**3**
Reviewed/supervised by:	**Anis Houaijia (DLR), Anton Meier (PSI), Christian Wieckert (PSI)**

Table of contents

1. Introduction

The conversion of solar energy into chemical energy carriers, e.g. solar hydrogen, represents an interesting pathway to the long-term storage of solar energy and the long-range transport from sunny and desert regions to the industrialized and populated centres of the earth. Solar fuels can burned to generate heat, further processed into electrical or mechanical work, or used directly to generate electricity in fuel cells and batteries to meet customers´ energy demand.

Solar fuels can be produced via direct or indirect processes using concentrated solar energy. Figure 1 shows different pathways for solar hydrogen production.

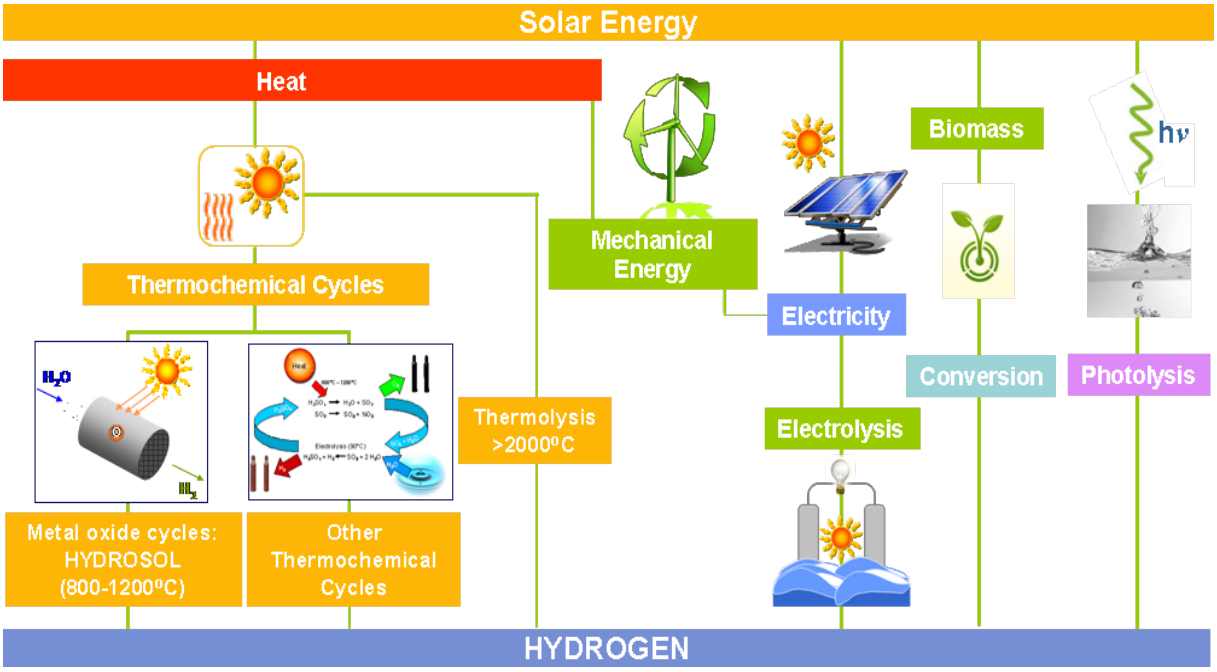

Figure 1: Pathways of solar hydrogen production processes.

Direct processes use the concentrated solar energy without intermediary energy conversions. The main pathway for the direct production of solar hydrogen from concentrated solar energy is the solar thermochemical path. The high temperature process heat is generated by concentrated solar energy and is directly introduced to a thermochemical process. The generated high temperature heat drives a series of chemical reactions that produce hydrogen [1]. The chemicals used in the process are reused within each cycle, creating a closed loop that consumes only water and produces hydrogen and oxygen. The necessary high temperatures are in the range of 500 to 2000° [2], [3]. Because a variety of thermochemical cycles is available, a screening will be performed and the most suitable thermochemical routes will be selected for further analysis within the techno-economic evaluation. The most

interesting representative of the indirect processes for solar hydrogen production is the high temperature electrolysis, which is more efficient economically than traditional room-temperature electrolysis because some of the total required energy is supplied as heat, which is cheaper than electricity, and also because the electrolysis reaction is more efficient at higher temperatures. Depending on the electrolysis technology and the stack configuration, the system operates between 100 and 850°C [4]. The leading technologies in the field of high temperature electrolysis, namely SOE (Solid Oxide Electrolysis) and MCE (Molten Carbonate Electrolysis) will be taken into consideration. Besides the thermochemical water splitting and the electrolysis processes, hydrogen production from carbonaceous feedstock will be investigated, namely solar steam reforming and solar biomass gasification. The analysis will also include innovative processes such as the solar low-temperature molten-salt heated reforming and the solar molten salt hydrothermal liquefaction of microalgae. Table 1 shows a summary of the processes, which will be studied within Task 9.4, and the responsible partners.

Table 1: Processes and responsible partners

Process	**Partner**
Solar high temperature electrolysis (SOE and MCE)	DLR, IMDEA, ENEA
Solar biomass gasification	DLR, CIEMAT, PSI
Solar thermochemical water splitting	DLR, IMDEA, CNRS, ABENGOA
Solar methane-steam reforming	DLR, CIEMAT
Solar low-temperature MS-heated reforming	ENEA
Solar MS-heated hydrothermal liquefaction of Microalgae	UNIPA, ENEA

2. Methodology of the technology assessment

Assessing technical and economic viability, the overall system analysis involves the three major steps listed in Figure 2. The overall system analysis consists of flowsheet elaboration, simulation of the process and economic analysis. This methodology will be applied to all hydrogen production processes in the framework of Task 9.4 in order to provide a better understanding of the system from a thermodynamic and economic point of view.

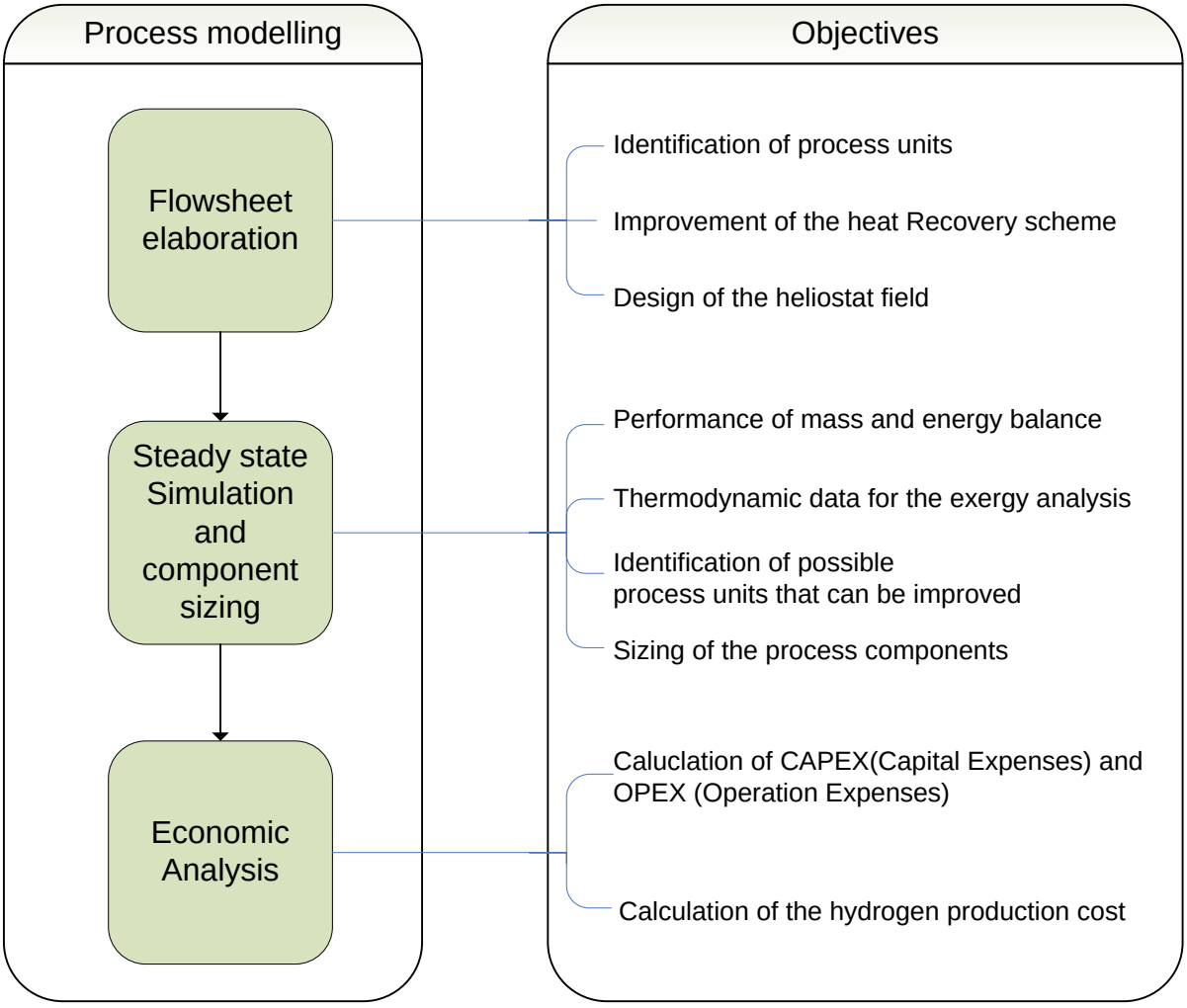

Figure 2: Methodology of the overall system analysis.

The overall system analysis starts with the layout of the solar part and the elaboration of the flowsheet in order to indicate the general flow of plant process streams and equipment. The flowsheet displays the relationship between the major equipment items of a plant facility. After elaboration of the flowsheet, the simulation of the process can be performed by using commercial tools such as Aspen Plus, Ebsilon Professional, Chemcad, etc. [5].

Aspen Plus and Ebsilon Professional have been selected as the appropriate software tools for the simulation of the processes, though other codes like Ecosimpro or Trnsys might be used if required. The behaviour of the system and its components can be modelled and analysed from a thermodynamic point of view. The simulation tools use the sequential modular approach regarding flow sheet elaboration. The various components are available in a library and can be linked by so-called connections, such as flow of mass or energy. The equations of the different components of the flow sheet will be solved sequentially. The simulation tools allow the calculation of energy and mass balances and provide the necessary inputs for the component sizing. Energy balances are performed on heats of reaction, heat capacities, expected temperatures and pressures at various points to calculate the amounts of heating and cooling needed in various places and to dimension the heat exchangers. Additionally, the overall performance of the processes will be analysed by calculating the solar-to-hydrogen efficiency.

The last step of the analysis consists of calculating the hydrogen production cost by taking into consideration the plant output and costs along its full lifetime. Calculations take into account the plant investment costs (CAPEX) as well as the operating costs (OPEX) [6]. The plant CAPEX is composed of the cost of conception and construction of the plant ("EPC cost") and the costs incurred by the plant owner to manage and insure the project, acquire the land, follow permitting process, etc. ("Owner costs"). At project stage, a plant cost estimate also includes provisions for contingencies that are intended to cover all cost sources not yet identified. The main contributors to the OPEX are the power consumption of electrical balance of plant (BoP) components such as pumps, compressors, etc. OPEX also includes the cost estimation of manpower, maintenance and insurance. The boundary conditions of the economic analysis, in terms of plant construction duration, discount factor, plant lifetime etc., will be defined by the WP9 partners in a further step. After that, cost reduction perspectives will be investigated. Several improvements can be expected, especially for the solar part across its main components. For example, the size of large heliostats is expected to increase up to 150 m². With this size increase, the total number of tracking system drives would decrease, reducing the tracking system costs per m². The heliostats are the most relevant cost factors for solar tower systems. Improvement in the dimensions for heliostats can yield a cost reduction of 7% per solar field area. Those cost reduction possibilities will be studied within a sensitivity analysis, which is normally performed at the end of the economic analysis.

This methodology will be applied to analyse each of the processes already defined by the WP9 partners, namely the solar steam reforming, the solar biomass gasification, the solar high temperature electrolysis and the solar thermochemical water splitting.

The system analysis of the mentioned processes will be carried out for two plant capacities, which are characterized by the hydrogen production rate. Two hydrogen production scenarios will be analysed within Task 9.4: (1) a hydrogen refuelling station and (2) an industrial process based on the last report published by the Fuel Cells and Hydrogen Joint Undertaking (FCH-JU) in February 2014 [7]. The proposed scenarios cover a wide range of plant

capacities depending on the further application of the hydrogen produced by the processes. Figure 3 summarises the hydrogen production scenarios and the specifications of each application. Each scenario is specified by the hydrogen production rate in kg/day, the end pressure of the hydrogen product, and the required purity.

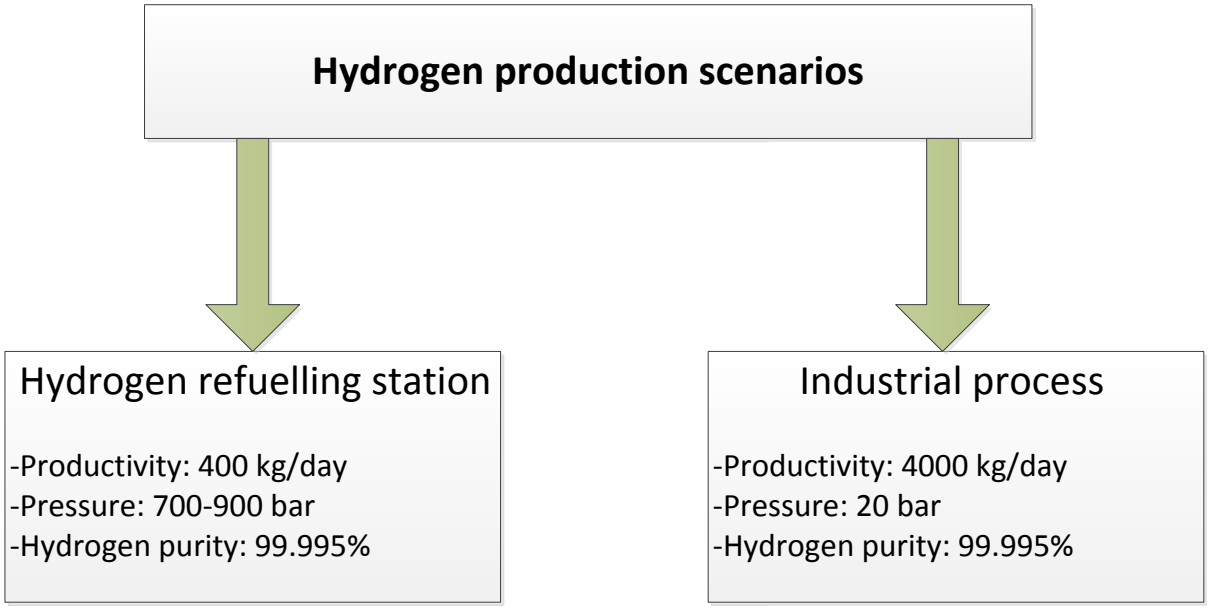

Figure 3: Summary of applications and use cases.

The first scenario consists of a small system for transport applications. It investigates the use of the produced hydrogen in hydrogen refuelling stations for fuel cell vehicles and buses. This scenario is characterized by a hydrogen production rate of 400 kg/day and an end compression up to 700-900 bar. The second scenario is a medium size system for industrial process applications with a capacity of 4000 kg/day and end compression of 20 bar.

3. Integration of the solar energy source

Solar energy concentrating technologies, being able delivering both heat and electricity, will be identified and investigated in order to assess their compatibility with the processes defined in Chapter 1.

3.1 Solar tower

The solar tower technology is a large-scale technology, which utilises many big, computer-controlled, sun-tracking mirrors, well known as heliostats, to focus sunlight on a receiver at the top of a tower. This receiver converts the solar radiation into heat. A heat transfer fluid (HTF) circulating in the receiver is absorbing the highly concentrated radiation reflected by the heliostats and converting it to thermal energy. Usually, the heat is coupled through a heat exchanger to a conventional steam cycle for producing electricity. This technology enables operation at high temperature and provides heat storage capacities. Solar towers typically are about 75-150 m high [8]. Such plants are best suited for utility-scale applications in the 10 to 200 MW_e range [9]. The solar tower technology is commercially available and provides high net solar-to-electrical efficiency. The process design of the plant depends on the HTF, which typically is water, molten salt or air. In this study, direct steam generation (DSG), molten salt (MS) and air-cooled solar towers are considered.

3.1.1 Air-cooled tower

Some European designs use air as heat transfer medium because of its high temperature and its good handiness. Another advantage of air as heat transfer medium is its free availability and non-toxicity. Moreover, air does not require freeze protection during times of non-operation. There are no special safety requisites and no environmental impact.

As an example, the 1.5 MW_e experimental and demonstration platform in Jülich, Germany (Figure 4) is the world's first solar thermal power plant using air as heat transport medium.

Figure 4: 1.5 MW_e solar tower in Jülich, Germany.

The receiver absorbing the concentrated solar radiation and transporting the heated air can be an open volumetric air receiver or a volumetric pressurized receiver. The *open volumetric receiver* is made of ceramic materials in a honeycomb structure. A fan sucks the air through absorbent pores and the air is heated up to temperatures between 650 and 850°C. On the front side, the incoming air is cooling down the receiver surface. Therefore, the volumetric structure produces the highest temperatures *inside* the receiver material, reducing the heat radiation losses on the receiver surface. Next, the air reaches the heat boiler, where steam is produced. Steam parameters may be up to 100 bar and 500°C, which is in the typical range for medium-sized conventional power plants. The steam generated there drives a turbine/generator and returns in form of condensate to the steam generator (Figure 5). The absorber modules made from SiSiC consist of an extruded parallel channel structure inserted into a cup. The inner surface of this structure is about 50 times larger than the aperture. The open neck of the cup is inserted into a double-walled steel casing, which is open to the hot air duct. Inside the casing, returning air is cooling the steel structure while being distributed and blown out to the receiver front between the individual absorber modules to be re-circulated through the receiver [10]. The thermal efficiency of the open volumetric receiver reactor is 76% ± 7% at 700°C under steady-state conditions. This technology has been then successfully proven in a number of projects during the last 25 years.

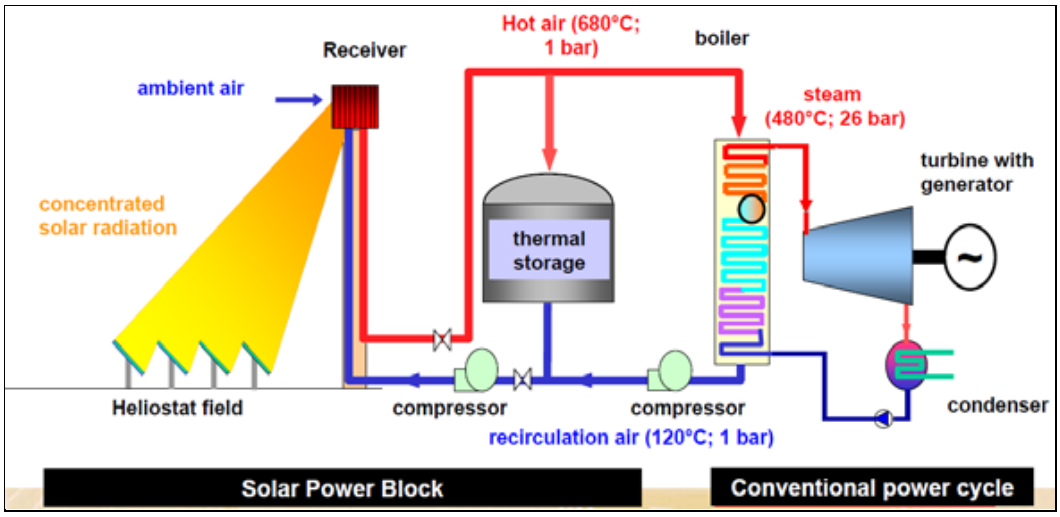

Figure 5: Scheme of air solar power tower.

In the case of the *volumetric pressurized receiver*, a compressor pressurises air to about 15 bars. A transparent glass dome covers the receiver and separates the absorber from the environment. The air is heated inside the pressurized receiver to temperatures of up to 1100°C, and driving a gas turbine connected to the compressor and the generator that produces electricity. The waste heat of the gas turbine goes to a heat boiler and additionally drives a steam-cycle process. Nevertheless, windows are critical and troublesome components since they must be relatively thin for minimum radiation attenuation, yet strong and durable at high temperatures and pressures. Quartz windows have an upper limiting temperature of 800°C and require active cooling.

The air-cooled solar power tower concept offers several benefits. Operation with steam parameters – as customary in conventional power plant engineering – ensures high efficiency and optimum use of the solar energy available. Major parts of the plant can be built using standard components from conventional power plant construction. Design, operation and maintenance concepts can benefit from the sound knowledge base from this sector and, consequently, a high operational reliability and availability can be expected. Solar-to-electric efficiency is estimated to be 13.5% [11].

A thermal energy storage (TES) system is connected in parallel to the boiler. The storage system at the solar tower in Jülich consists of a rectangular housing of 7 m x 7 m x 6 m size. The storage is partitioned into four chambers of identical size, connected in parallel through a dome and connecting pipes. Each of the chambers is filled with a ceramic storage material formed to provide a large heating surface. The total volume of the inventory amounts to 120 m^3. The steel containment is protected from the storage heat and kept at a surface temperature below 60°C through an inner insulation made of ceramic fibre blankets. With this storage type, air is in direct contact with the solid storage medium and exchanges heat as it flows along a flow-path through the storage medium. When charging, hot air passes through the

vessel filled with ceramic material, which develops a temperature profile between the hot and the cold end of the storage. The cool air exiting the steam generator and/or storage is returned to the receiver. To discharge the storage, cool air from the steam generator is circulated in reverse flow through the storage vessel and back to the steam generator [12]. However, for the air-cooled solar tower using the pressurized volumetric receiver, storage is available only for transient operation.

3.1.2 Direct steam generation

In the direct steam generation (DSG) solar tower technology, water is used as heat transfer fluid and thus may be sent directly to the turbine generator. Using water as the heat transfer medium has the advantage of being low cost and neither flammable nor harmful to the environment. As an example, the PS-10 solar power tower (Figure 6), works on a saturated steam concept: it stores heat in tanks as superheated and pressurized water at 50 bar and 285°C. The water evaporates and flashes back to steam, when pressure is lowered. The solar radiation is concentrated onto the solar receiver, which produces saturated steam at 40 bar 250ºC. This receiver has a cavity design to reduce radiation and convection losses. The steam is sent to the turbine, where it expands, producing mechanical work and electricity. The turbo-generator output goes to a water-cooled 0.06 bar pressurized condenser. The condenser output is preheated by 0.8 bar and 16 bar turbine extractions. The output of the first preheater is sent to a deaerator fed with steam from another turbine extraction. A third and last preheater is fed with steam coming from the receiver. This preheater increases the water temperature to 245ºC. This flow is mixed with the flow of water returning from the drum, raising the temperature of water fed to the receiver to 247ºC. PS-10 achieves an annual efficiency of 14.4% in conversion from intercepted solar energy to electricity [13].

Figure 6: 11 MW_e saturated steam PS-10 plant in Seville, Spain.

Recently, the Sierra Sun Tower pilot plant has been built, working with superheated steam at 440ºC and 60 bar. It consists of 16 receiver/heliostat field modules generating superheated

steam to power a single 46 MW_e turbine [14]. BrightSource has also built up the Ivanpah Solar Power Complex, which consists of three superheated steam plants that work with steam at 560ºC and 160 bar. Each plant has a re-heat steam turbine of 123 MW_e, with a total nominal capacity of 370 MW_e.

3.1.3 Molten Salt Solar Tower

In a molten salt (MS) solar tower, the solar receiver converts the collected solar radiation into heat using molten salt as heat transfer fluid. Usually, the molten salt is a mixture of 60 wt% sodium nitrate and 40 wt% potassium nitrate ("solar salt"). There exist several types of molten salts, of which nitrate compositions are popular having low melting points [15], but their boiling (decomposition) points are also low in the range 600-650°C. Carbonate salts allow for higher end temperatures, but are corrosive and have high melting points. Thus, nitrate-based mixtures so far remain the state-of-the-art choice.

US designs – such as the 10 MW Solar-Two power tower (Figure 7) – utilize molten nitrate salt because of its superior heat transfer and energy storage capabilities. Moreover, the molten salts are not toxic and compositionally stable over an extended period when properly protected from the environment and from overheating.

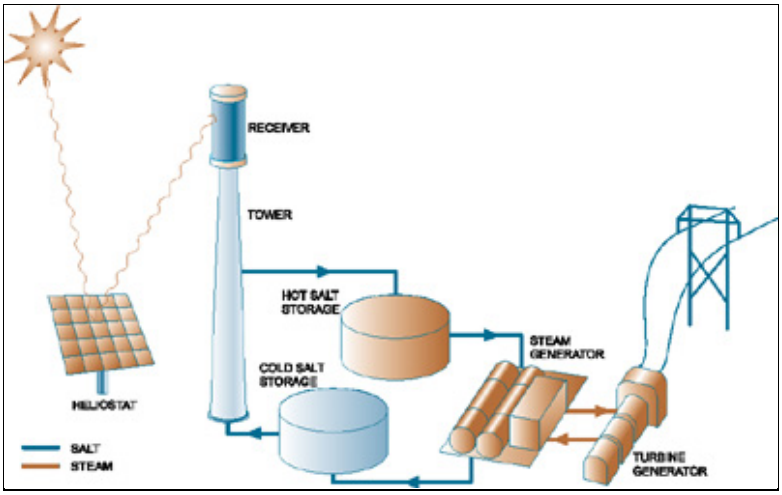

Figure 7: Schematic of the molten salt solar tower.

Thanks to the long-term molten salt thermal storage system that is normally integrated in this kind of plants, it is possible to operate round-the-clock in summertime. Indeed, molten salts are suitable for long-term storage over many hours due to their high thermal density and fluid properties at high temperature. When molten salts act as both heat transfer fluid and thermal energy storage, the need for a heat exchanger is eliminated, the overall plant efficiency is improved, and the cost are lowered. Usually, a two-tank storage system consisting of a "cold"

and a “hot” tank is included in the solar tower power plant. The molten salts from the “cold” tank are flowing through the solar receiver, heated up and sent to the “hot” tank. As the steam generator is fed independently from the hot tank, the thermal storage system works as a buffer during solar transients and periods of no insolation, so that the steam turbine working conditions are stable. Thus, the first commercial molten salt power tower plant Torresol Gemasolar can supply 15-hours of full-load-equivalent heat storage capacity for a plant capacity of 17 MW_e [16].

3.2 Parabolic Trough Collector

Parabolic-trough collectors (PTC) are linear-focusing concentrating solar devices suitable for working in the 150-400ºC temperature range [17]. Current research with new thermal fluids intends to increase the operating temperature up to 500ºC [18]. Concentrated solar radiation heats the fluid that circulates through the receiver tube, thus transforming the solar radiation into thermal energy in the form of sensible heat of the fluid. Figure 8 shows a typical PTC and its main components.

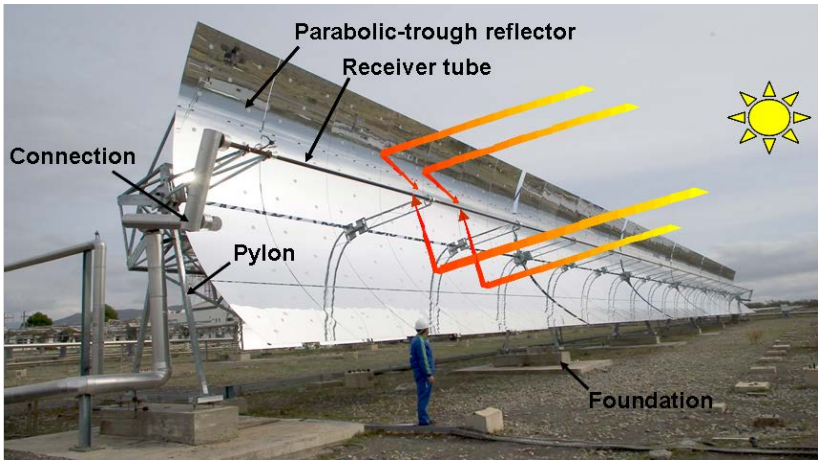

Figure 8: Typical parabolic-trough collector.

Collector rotation around its axis requires a drive unit. One such drive unit is usually sufficient for several parabolic-trough modules connected in series and driven together as a single collector. Drive units composed of an electric motor and a gearbox are used for small collectors (aperture area < 100 m2), while powerful hydraulic drive units are required to rotate large collectors. At present, all commercial PTC designs use a single-axis sun-tracking system [19] consisting of a local control unit for each drive unit placed on the central pylon.

Commonly, thermal oils are used as the working fluid in PTCs for temperatures above 200ºC, because at these operating temperatures normal water would produce high pressures inside the

receiver tubes and piping. Such high pressure would require stronger joints and piping, and thus raise the cost of the collectors and the entire solar field. However, the use of demineralized water for high temperatures and pressures is currently under investigation, and the feasibility of direct steam generation (DSG) at 400ºC and 100 bar in the receiver tubes of PTCs has already been proven in an experimental stage [20]. For temperatures below 200ºC, either a mixture of water and ethylene glycol or pressurized liquid water can be used as the working fluids because the pressure required in the liquid phase is moderate. The oil most widely used in PTCs for temperatures up to 395ºC is VP-1, which is a eutectic mixture of 73.5% diphenyl oxide and 26.5% biphenyl. The main problem with this oil is its high solidification temperature (12ºC), which requires an auxiliary heating system when oil lines run the risk of cooling below this temperature. Since the boiling temperature at 1013 mbar is 257ºC, the oil circuit must be pressurised with nitrogen, argon or some other inert gas when oil is heated above this temperature. Though there are other suitable thermal oils for slightly higher working temperatures with lower solidification temperatures, they are too expensive for large solar plants.

The typical PTC receiver tube is composed of an inner steel pipe surrounded by a glass tube to reduce convective heat losses from the hot steel pipe. The steel pipe has a selective high-absorption (>90%), low-emission (<30% in the infrared) coating that reduces radiative thermal losses. Receiver tubes with glass vacuum tubes and glass pipes with an anti-reflective coating achieve higher PTC thermal efficiency and better annual performance, especially at higher operating temperatures. Receiver tubes with no vacuum are usually used for working temperatures below 250ºC, because thermal losses are not so critical at these temperatures. Due to manufacturing constraints, the maximum length of a single receiver pipe is less than 6 meters. Thus, the complete receiver tube of a PTC is composed of a number of single receiver pipes welded in series up to the total length of the PTC that is usually within 100–150 meters. Two PTC designs specially conceived for large solar thermal power plants are the LS-3 (owned by the Israeli company SOLEL Solar Systems) and EuroTrough (owned by the EuroTrough Consortium), both of which have a total length of 100 m and a width of 5.76 m, with back-silvered thick-glass mirrors and vacuum absorber pipes. The American Solargenix design has an aluminium structure. Other collector designs are becoming commercially available in the short-to-medium term like the ones developed by the companies Solargenix, Albiasa or Sener. The main constraint when developing the mechanical design of a PTC is the maximum torsion at the collector ends, because high torsion would lead to a smaller intercept factor and lower optical efficiency.

The suitable PTC temperature range and the good solar-to-thermal efficiency up to 400ºC make it possible to integrate a parabolic-trough solar field in a Rankine water/steam power cycle to produce electricity. Figure 9 shows the simplified scheme of a typical solar thermal power plant using parabolic-troughs integrated in a Rankine cycle. At present, the HTF technology commercially available for parabolic-trough power plants is based on oil as the heat carrier between the solar field and the power block.

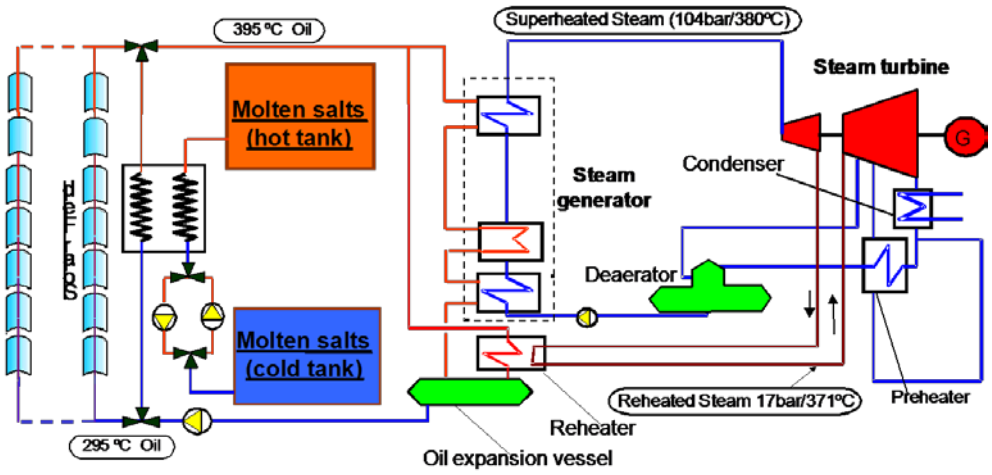

Figure 9: Scheme of a parabolic trough plant introducing a molten-salt circuit with two storage tanks to increment the capacity factor.

Although parabolic-trough power plants usually have an auxiliary gas-fired heater to produce electricity when direct solar radiation is not available, the amount of electricity produced with natural gas is always limited to a reasonable level. This limit changes from one country to another: 25% in California (USA), 15% in Spain, and no limit in Algeria. Typical solar-to-electricity efficiencies of a large solar thermal power plant (>30 MW_e) with parabolic-trough collectors is between 15% and 22%, with an average value of about 17%. The yearly average efficiency of the solar field is about 50%. The commercial maturity and reliability of PTC systems has been confirmed by the Solar Electricity Generating Systems (SEGS) with over 2.2 million square meters of collector area and daily operation using thermal oil as the working fluid (HTF technology). SEGS II to IX were designed and implemented by the LUZ International Ltd. company from 1985–1990. All SEGS plants are located in the Mojave Desert, northwest of Los Angeles (California, USA). Their plant availability is over 98% and their solar-to-electricity annual efficiency is in the range of 14–18%, with a peak efficiency of 22%. Thanks to the continuous improvements in the SEGS plants, the total SEGS I cost of \$0.22/kWh_e for electricity produced was reduced to \$0.16/kWh_e in the SEGS II and down to \$0.09/kWh_e in SEGS IX by the year 1996 [21].

With the revival of commercial Solar Thermal Electricity (STE) projects since 2006 in Spain and the United States, a new generation of SEGS-type plants have come to the arena. This is the case of the Nevada Solar One (NSO) project of 75 MW_e in US, the Ibersol project in Puertollano, Spain, or the Shams One 100 MW_e plant in Abu Dhabi [22]. Nevada Solar One started grid-connected operation in June 2007 and is considered a milestone in the opening of the second market deployment of PTC technology in the world after the SEGS experience. Since then more than 40 PTC plants (about 50 MW_e each) were built in Spain and more than 2 GW_e in the US, demonstrating routine operation. The main characteristics of the NSO plant are shown in Table 2.

Table 2: Main characteristics of Nevada Solar One (NSO) plant

SOLAR FIELD		**POWER BLOCK**	
Solar Collector Assemblies	760	Turbine Generator Gross Output (MW_e)	75
Aperture Area (m)	5	Net Output to Utility (MW_e)	72
Aperture Area (m^2)	470	Solar Steam Inlet Pressure (bar)	86.1
Length (m)	100	Solar Steam Reheat Pressure (bar)	19.5
Concentration Ratio	71	Solar Steam Inlet Temperature (°C)	371
Optical Efficiency	0.77		
Number of Mirror Segments	182,400		
Number of Receiver Tubes	18,240		
Field Aperture (m^2)	357,200		
Site Area (km^2)	1.62		
Field Inlet Temperature (°C)	300		
Field Outlet Temperature (°C)	390		

In spite of their environmental benefits, there are still some obstacles to the commercial competitiveness of the PTC technology. The main barriers at present are the high investment cost (2,500–5,000 $/kW, depending on plant size and thermal storage capacity) and the minimum size of the power block required for high thermodynamic efficiency. However, these barriers are shared by all solar thermal power technologies currently available [23].

One of the strategies to increase the capacity factor of the power block and to mitigate risk perception is to integrate a parabolic-trough solar field in the bottoming cycle of a combined-cycle gas-fired power plant. This configuration is called the Integrated Solar Combined Cycle System (ISCCS). Although the contribution of the solar system to the overall plant power output is small (10–15% approx.), the ISCCS seems a good approach to market penetration in some developing countries. The Government of Algeria has promoted an ISCCS plant and the World Bank, through its Global Environment Facility (GEF), funded ISCCS plants in Morocco and Egypt [24]. Similar schemes are being promoted in other countries of the MENA region.

In many countries, the market penetration of STE systems is based on feed-in-tariffs or green certificates linked to significant restrictions or regulations regarding the use of hybrid concepts like ISCCS schemes. Consequently, the use of thermal energy storage systems with an oversized solar field is pursued to optimize economics and dispatchability of PTC plants.

For temperatures up to 300ºC, thermal mineral oil can be stored at ambient pressure, and is the most economical and practical solution. Synthetic and silicon oils, available for up to 410ºC, have to be pressurized and are expensive. Molten salts can be used between 220 and 560ºC, at ambient pressure, but require parasitic energy to keep them liquid.

Two pioneering projects introducing thermal storage are the plants Andasol-I and Andasol-II [25]. These PTC plants installed in Guadix, Spain, have a nominal power of 50 MW_e each and an oversized solar field (510,120 m^2 mirror surface area) with an integrated 1,010 MW_{th}

molten-salt thermal storage system to extend the plant's full-load operation 7.5 hours beyond daylight time, leading to a capacity factor of 41%. Figure 9 shows a simplified Andasol plant flow diagram and Figure 10 an aerial view of the tanks. As can be observed, the introduction of a third circuit with molten salts adds more complexity with a number of new heat exchangers and additional heat tracing to avoid the salts thawing. It is still too early to know implications in terms of energy management and operational robustness. Preliminary operational data demonstrate the capacity of the plant to supply electricity several hours after sunset. Other countries such as Italy are planning further steps with the use of molten salts, both for thermal storage and solar field, like the 5-MW_e demonstration project Archimede [26].

Figure 10: Aerial view of the Andasol plant in Guadix, Spain, showing the power island (insert) and details of molten-salt storage tanks and heat exchangers.

Even though molten salts nowadays are the preferred storage technology for demonstration and first commercial projects in the US and Spain, alternative options are under development and assessment, such as concrete or other solid bed materials [27] and phase change media (PCM) [28]. PCM provide a number of desirable features, e.g. high volumetric storage capacities and heat availability at constant temperatures. Energy storage systems using the latent heat released on melting eutectic salts or metals have often been proposed, but never carried out on a large scale due to difficult and expensive internal heat exchange and cycling

problems. Heat exchange between the heat transfer fluid (HTF) and the storage medium is seriously affected when the storage medium solidifies. Encapsulation of PCMs has been proposed to alleviate this problem. Combining the advantages of direct-contact heat exchange and latent heat, hybrid salt-ceramic phase change storage media have been proposed recently. The salt is retained within the submicron pores of a solid ceramic matrix such as magnesium oxide by surface tension and capillary force. Heat storage is then accomplished by two modes: (1) the latent heat of the salt and (b) the sensible heat of the salt and the ceramic matrix [29].

PCMs are extremely suitable for direct steam generation PTC plants. If the superheated steam required to feed the steam turbine in the power block were produced directly in the receiver tubes of the PTCs, the oil would be no longer be necessary, and temperature limitations as well as environmental risks associated with the oil would be avoided. Simplification and cost reduction of the overall plant configuration is then evident since only one single fluid is used. This effect, combined with the increase in efficiency after removing intermediate heat exchangers, might lead to a 15% cost reduction of the electricity produced. The disadvantages of this concept originate from thermo-hydraulic problems associated with the two-phase flow in the evaporating section of the solar field. An additional disadvantage is the use of much heavier absorber tubes and interconnecting lines required for the high-pressure steam. Nevertheless, experiments performed in a 2-MW_{th} loop at the Plataforma Solar de Almería (PSA) in Spain have proven the technical feasibility of direct steam generation with horizontal PTCs at 100 bar and 400ºC [30].

3.3 Linear Fresnel Reflector

Conceptually, a Linear Fresnel Reflector (LFR) is an optical analogue of the Parabolic Trough Collector (PTC) technology. It consists of 2-D concentrating reflectors with linear focus. In this case, the parabolic reflective surface is obtained by an array of linear mirror strips, which independently move and collectively focus on the absorber, see Figure 11 and Figure 12. Reflective segments are placed close to the ground, while absorber lines are suspended from elevated towers [31]-[32]. The solar field is composed of several parallel rows of such collectors aligned on a north-south horizontal axis, tracking the sun from east to west to ensure that solar radiation is continuously focused on the linear receiver. This configuration allows for small distances between collector rows increasing the use of ground area from 33% in PTC to about 60-70% in LFR systems. However, optical quality is lower in comparison with PTC because of higher influence of the incidence angle and the cosine factor.

The objective of LFR plants is to reproduce PTC performance but at lower costs. LFR optimizes material and cost and simplifies the construction thanks to the use of low-cost flat float glass reflectors, direct steam production, lower cost non-vacuum thermal absorbers, light reflector support structures close to the ground and lower O&M costs due to easier access to primary reflectors.

In the past, the focus was on the production of saturated steam at 270ºC, because the non-vacuum absorber tubes have low efficiency at high temperature, as shown in the solar plant scheme in Figure 13. Recently, AREVA and NOVATEC have developed new absorbers able to work at temperatures above 450ºC. With such a development, according to developers, LFR would be expected to operate with superheated steam at 450-500 °C, yielding an efficiency improvement of up to 18.1% relative to current saturated steam operation at 270°C [33].

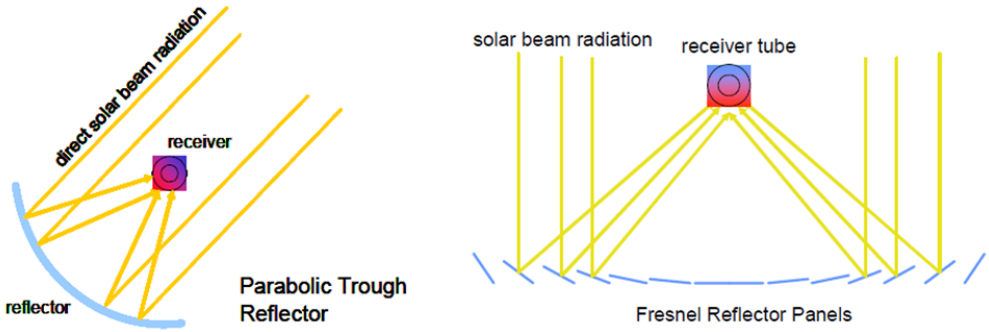

Figure 11: Optical fundamentals of LFR versus PTC.

Figure 12: Novatec's Puerto Errado 2 (PE2), a 30 MW solar thermal power station in operation since August 2012 in Spain.

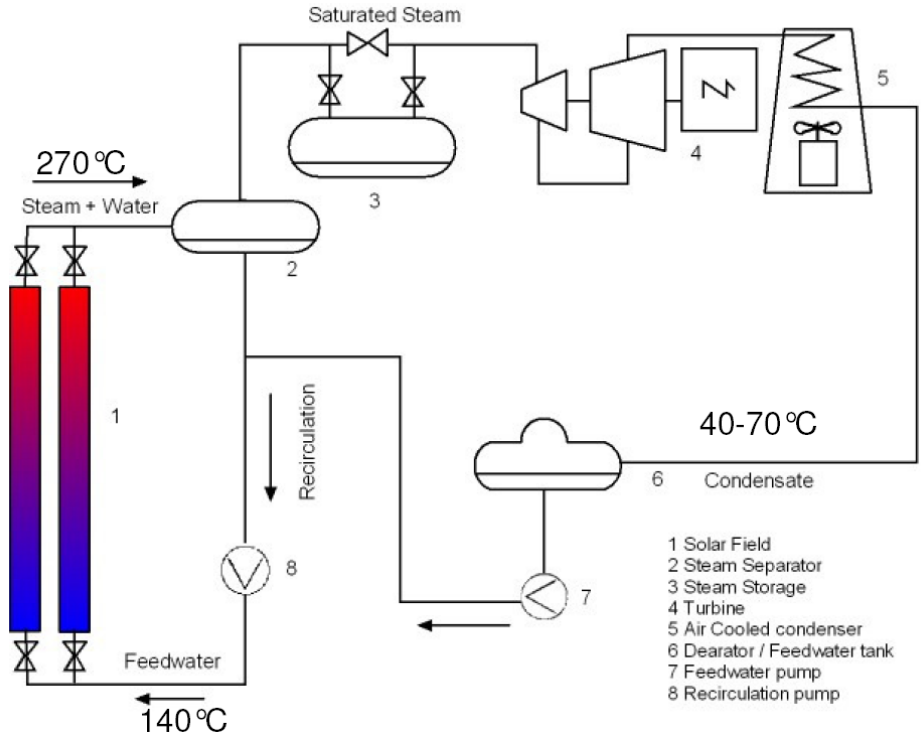

Figure 13: NOVA-1 plant scheme with direct steam generation [34].

Other heat transfer fluids are also possible in the solar loop of LFR. Recently, companies like FRENELL are proposing the so-called direct molten salt (DMS) technology (Figure 14). It makes direct use of molten salts in the solar loop heating up to 550ºC and therefore allows for heat storage and generation of superheated steam [35].

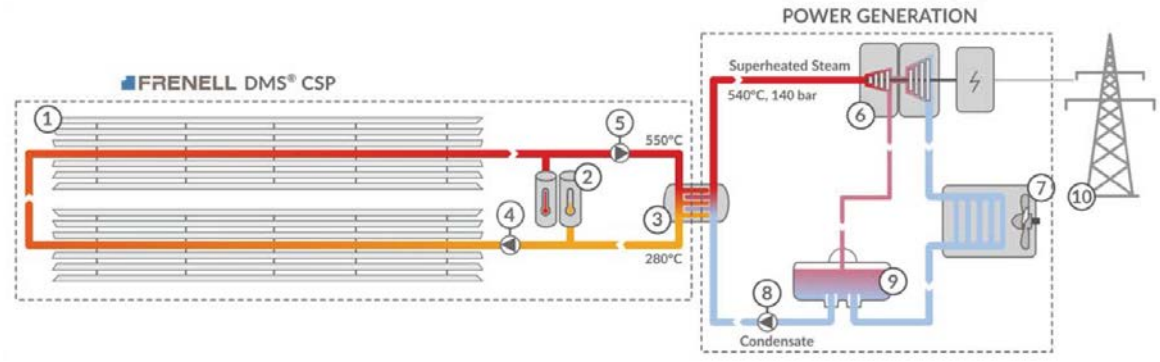

Figure 14: Direct molten salt Linear Fresnel system with storage and dispatchable power generation [35].

4. Process Flow charts for the scaled-up plants

4.1 Solar low temperature MS-heated reforming

Steam reforming of natural gas (NG) is currently the most widely used process for hydrogen production. Conventional steam reforming processes are carried out at temperatures above 800°C in externally heated tubular reactors and the reaction heat duty is provided by placing the reactor tubes inside fossil fuel furnaces. Several economic and environmental advantages could be obtained by lowering the operating temperature below 565 °C. These include the use of lower grade materials, reduced overall process heat requirements and the possibility to provide the heat of reaction with concentrating solar thermal (CST) plants using the so-called solar salt, i.e. a binary molten salt (MS) mixture of $NaNO_3$ and KNO_3 (60%/40% w/w), as heat transfer fluid. As reported in Section 3.2, such type of installations can rely on the only commercial heat storage solution available to date for CST plants; this is a very important feature, especially when the CST plant must provide process heat. Indeed, heat storage ensures a smoother and extended heat supply to the chemical plant, potentially attaining round-the-clock solar operation with the appropriate design and insolation conditions. Consequently, the operation of the chemical plant is more stable and its capacity factor dramatically improved.

Recently, an innovative steam-reforming reactor has been developed and tested within the CoMETHy project, both at laboratory and pilot scale [36]. Such reactor was designed for the low-temperature (450-550°C) steam reforming of several carbonaceous feedstocks like methane, biogas and (bio)ethanol using a MS stream at 550-565°C as heat transfer fluid to provide the process heat.

The reactor has a shell-and-tube configuration, where the MS stream flows in the shell-side. Reaction tubes are immersed in the MS flow and are composed by two coaxial elements: an external steel tube, which is in direct contact with molten salts, and an internal cylindrical hydrogen-permeable membrane. A sweep gas such as steam is fed inside the membrane (permeate space) in counter-current flow to enhance hydrogen permeation.

By continuously removing hydrogen from the reaction space, the integrated membranes allow to push the conversion of the feedstock beyond the low values that could be obtained with conventional reformers at such low temperatures. The system analysis for low-temperature MS-heated reforming is based on a membrane reactor such as the one described above – or a similar configuration as discussed later – and is considering CH_4 as reformable feedstock.

In the process analysis, the solar reforming (SR) plant is assumed to operate continuously using heat from the hot MS stream coming from the solar plant. When solar energy is not available and the heat storage of the CST plant is depleted, a backup fuel-fired heater is used to heat the molten salt [37].

Two main process configurations were analysed:

- **Retentate recirculation:** in this configuration, the retentate at the outlet of the reactor is compressed and recycled to the reactor's feed after CO_2 removal; the heat duty of the reactor is entirely provided by the MS stream, which is heated either by the CST plant or by a backup burner.
- **Retentate burning:** in this configuration, the retentate containing CH_4 and H_2 is burned to provide a part of the heat duty of the reactor, while the remaining part is provided by the hot MS stream.

Only solutions with retentate recycling will be considered here, and two further cases were studied:

- **Power export:** Molten salts provide heat only for the chemical process (reactor heat duty and generation of process steam) and for the generation of superheated steam to be used in a power cycle. The excess power produced is exported to the grid.
- **No power export:** Molten salts provide heat only for the chemical process.

Two different reactor architectures were assumed for two different plant capacities (Figure 15): (1) an integrated membrane reformer (such as the one previously described) for the 1,500 Nm^3/h (3.2 t/d) and (2) a multi-stage reformer with inter-stage membrane separation of hydrogen for the 5,000 Nm^3/h (10.8 t/d) plant. The reason for this choice is that the non-integrated configuration appears as more suitable for larger capacity reactors.

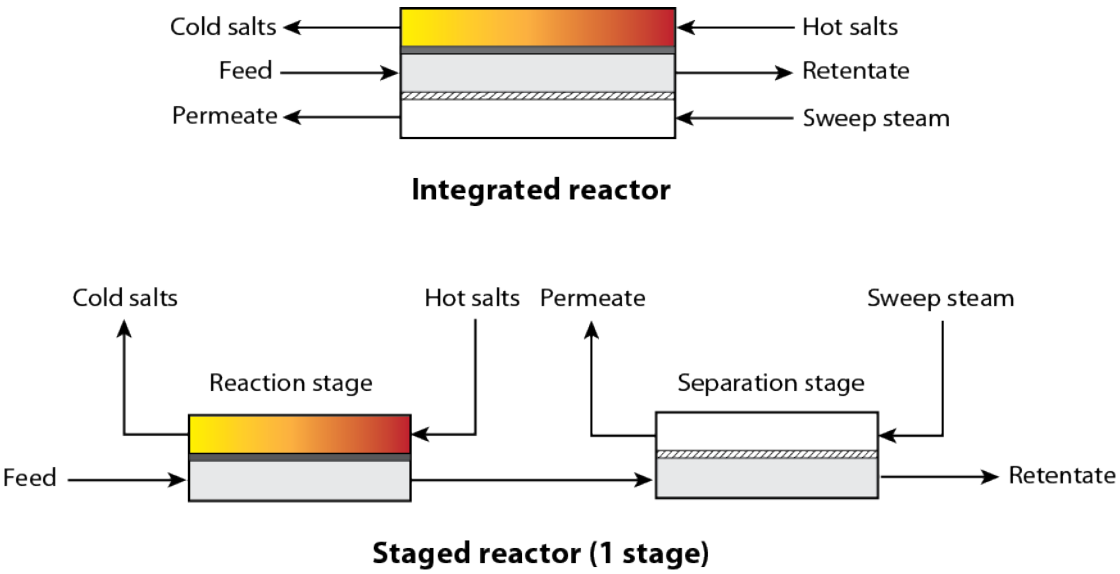

Figure 15: Conceptual schemes of the integrated (top) and staged (bottom) membrane reformer (only one stage is represented for the staged configuration).

Figure 17 shows the reference process flow chart for the retentate recirculation scenario with power export. The solar plant, which includes the solar field and the thermal energy storage

system, is designed to heat and store MS up to a temperature of 550°C. Molten salts are fed to the SR section (blue shaded circle in Figure 16). The MS temperature at the outlet of the reaction section is around 490°C. Since cold salts are stored at 290°C, the residual MS heat is used to produce the process steam required for the SR reaction and the sweeping steam for the membrane separation stages; additional steam is produced and used to generate power in a steam turbine. Excess electrical power is exported to the grid.

The NG is mixed with steam and sent to the reaction section, which operates at about 540°C and 10 bar. Hydrogen recovered by the membrane units is compressed up to 20 bar. The retentate, which contains unreacted CH_4 and a few mole percent of H_2O, CO_2 and CO produced by the reaction, as well as H_2 not separated by the membranes, is initially cooled down and the heat recovered is used to generate steam. Subsequently, CO_2 is removed by a conventional amine absorption process, and the remaining stream is compressed and recirculated to the feed of the SR section.

When the cost of electricity is low, a second option can be considered, which excludes power export. In this case, the steam generator/superheater placed downstream of the reforming section is substituted with a lower duty steam generator, which produces only low pressure and process steam. As a result, the temperature of the MS stream returned to the cold storage tank is about 400°C, and the thermal duty of the solar plant is about 40% lower compared to the scenario including power export.

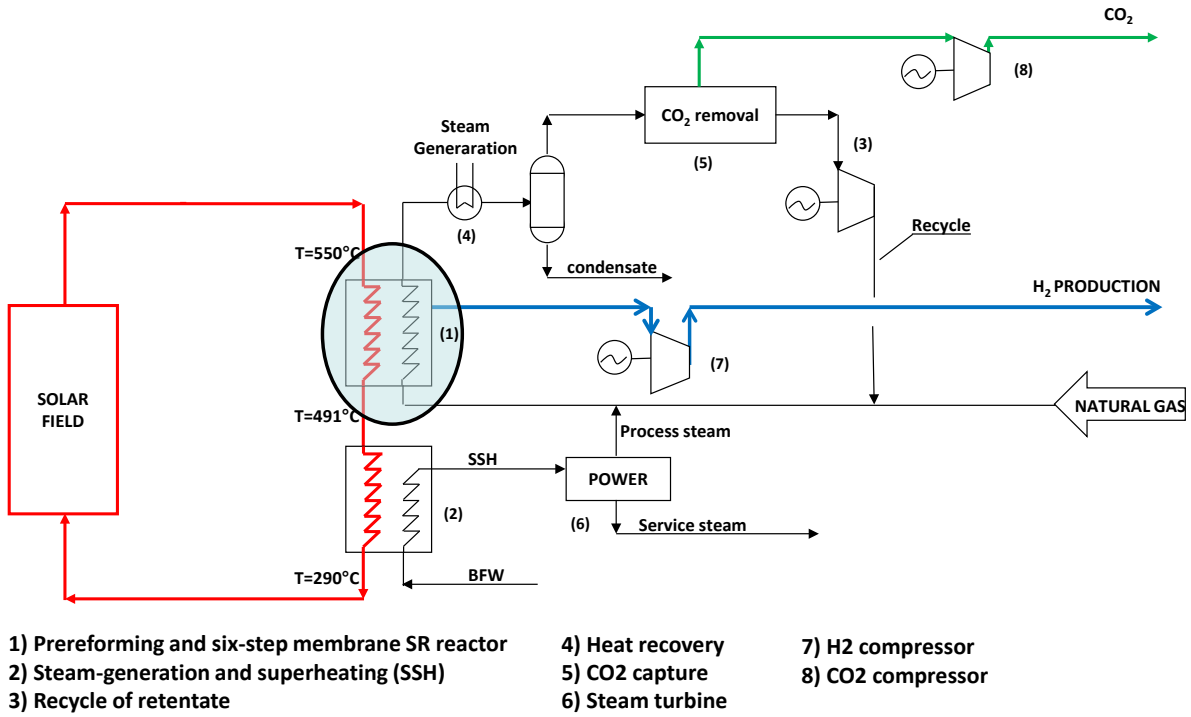

Figure 16: Process flow chart for low temperature MS-heated reforming ("retentate recirculation" scenario with power export).

4.2 Solar MS-heated hydrothermal liquefaction of microalgae

In this study, the utilization as heat transfer fluids of a ternary mixture of $Ca(NO_3)_2/NaNO_3/KNO_3$ (43/42/15 w/w) of molten salts was considered. This salt mixture can work in the temperature range 290-420°C that is quite compatible with the temperature adopted for the hydrothermal liquefaction (HTL) process and characterized by a melting temperature as low as 120°C, which allows a more economic start-up of the solar plant.

The coupling of a CSP plant – using molten salts as HTF – with a plant for hydrothermal liquefaction of microalgae, was studied under the constraint of maximizing thermal recovery from the hot reactor effluent (Figure 17). The goal was to detect the most critical section of the system from the techno-economic point of view and to estimate the minimum selling price of the produced biocrude to compare it with the cost of similar stream produced using conventional processes.

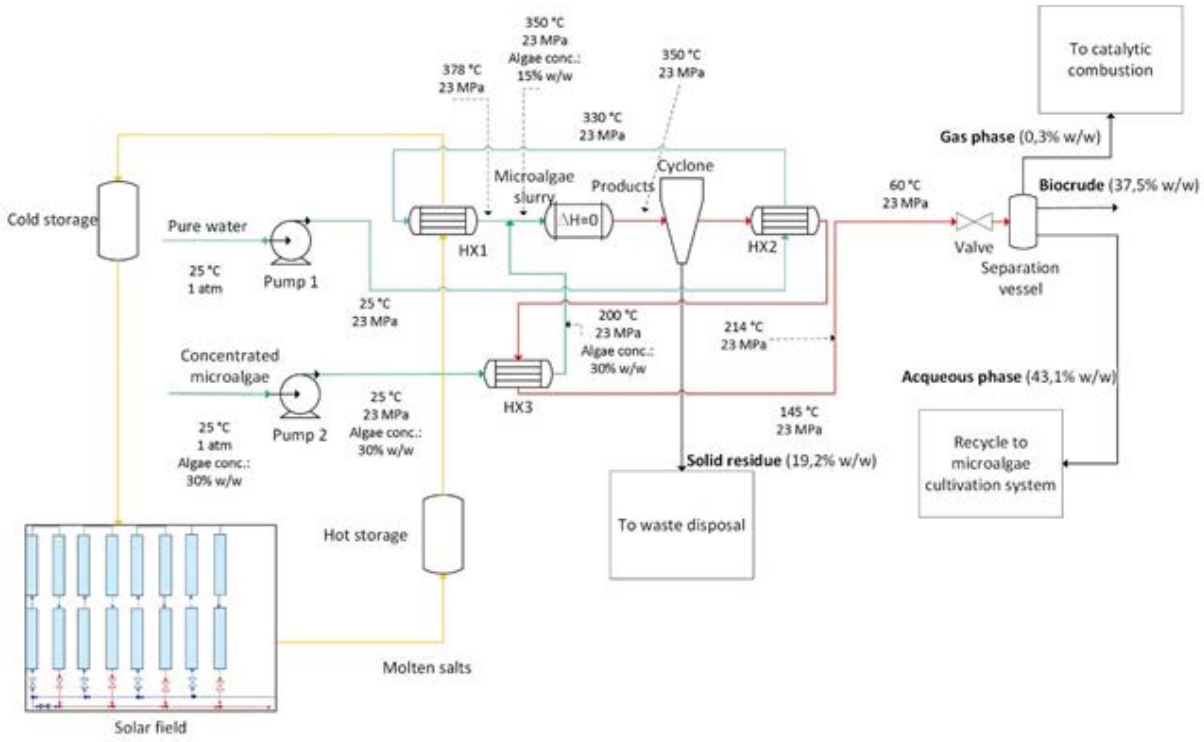

Figure 17: Schematic description of the solar assisted hydrothermal liquefaction process.

All calculations were performed using Matlab® and Microsoft Excel®. Thermodynamic and transport properties of water were obtained using XSteam software. Mass and energy balances were conducted in order to determine the energy inputs and outputs of the process; this information was used to design the main equipment (reactor and heat exchangers). The required power input, the physico-chemical and transport properties of the thermal fluid – as well as its temperature variation between inlet and outlet of the solar field – were used to calculate the number of solar collectors and their layout.

In order to compute the yield of the products of HTL processing of microalgae, the kinetic model proposed by Valdez and Savage [38] was used, where the biomass is modelled as a mixture of the three main biochemical constituents (proteins, carbohydrates, and lipids) and ashes, the latter being considered as an inert.

The estimation of capital cost for the HTL section of the plant was performed using Guthrie's method, where the capital expenditure (CAPEX) is estimated as a function of the cost of each single equipment of the plant. The equipment cost was estimated from correlations found in the literature [39]-[40] that relate the equipment cost with its size (Table 4). The bare module cost (BMC; Table 3), i.e. the total cost to install each equipment taking into consideration labour cost, insurance, general expenses, etc., was estimated by multiplying the cost of equipment purchased by a suitable correction factor considering that apparatus were built in AISI 316 stainless steel and rated to work at high pressure.

Based on previous projects, ENEA staff estimated the cost of the solar field, which was considered the CAPEX for the solar field. The CAPEX of both the HTL section and the solar field was summed to obtain the value for the full plant.

The operating expenditure (OPEX) comprises the costs associated with raw materials, waste disposal, utilities, labour and others. It was estimated from correlations reported by Peters *et al.* [40] using the CAPEX, the number of equipment pieces, as well as mass and energy flow. The purchase cost of microalgae was considered to be 0.3 €/kg [41] and the cost of electricity was assumed 0.173 €/kWh; the cost of disposal of aqueous phase products was neglected, as it was presumed that these products were recycled back to the microalgae cultivation system. The working capital, i.e. the amount of money required to make operative the plant, was assumed 20% of the CAPEX.

Table 3: Bare module cost of process units constituting the HTL plant.

Equipment	**C_{BM}[1] [€]**
HX1	264,000
HX2	201,000
HX3	203,000
Slurry pump (2 units)	207,000
Pure water pump (2 units)	333,000
Reactor	500,000
Cyclone	140,000
Separation vessel	145,000
Total HTL Plant	2,554,000

[1] Bare module cost (C_{BM}) of the equipment referred to Euros (2014), chemical engineering plant cost index (CEPCI) equal 579.8.

Table 4: Costs of the solar plant

Item	**Components**	**Cost (€)**
Solar field	Solar Collectors	616,667
	Receiver tubes	150,000
	Molten salts pump	240,000
	MS piping	116,667
	MS piping rack	23,333
	Electrical bulk materials	28,125
Thermal Energy Storage (TES): 2 Tanks	TES molten salts tank	115,956
	Steel structure for MS tank	120,000
	Melter	60,000
	Electrical heaters for TES	15,000
	Molten salts	41,363
Back up heater (powered by biocrude)	Back up heater (MSH) incl. fans	235,704
Other	Demi unit package	29,063
	Demi water tank	4,500
	Air compressor	7,500
	Instrumentation for measurement & control	210,038
	Control room	30,000
	Insulation & paintings	26,250
	Installation	174,856
	Transports	80,043
TOTAL (1) =		***2,325,063***
	Civil works	187,500
	Engineering + overhead + profit	875,133
	Contingency	1,076,141
TOTAL (2) =		***2,138,774***
TOTAL (1+2) =		**4,463,837**

In order to estimate the minimum fuel-selling price (MFSP) of the biocrude, a cash flow analysis was performed. A plant lifetime of 25 years was assumed with production starting from the 3rd year, while the first two years are dedicated to the construction of the plant; the interest rate on the investment was taken to be 10% and the taxation rate on revenue 40%. The MFSP was calculated with the Excel solver by imposing the net present value (NPV) of the project at the end of its life to be equal to zero.

By optimization of thermal integration among the hot stream recovered from the hydrothermal reactor and the two cold streams fed to the process it was found that the solar

field should supply the reactor with a thermal power of 800 kW necessary to heat the water in heat exchanger HX1 from 330°C to 378°C.

By hypothesizing a temperature difference of 30°C and 10°C for the outlet and inlet section of HX1, respectively, molten salts must enter the solar field at 340°C to be heated up to 410°C. The best compromise between the solar fraction of energy used by the process and the amount of biocrude used as energy back-up to ensure continuous operation of the plant also in the absence of solar radiation was obtained considering a solar plant constituted by 3 strings of parabolic solar collectors each 200 m long.

By this choice, the solar fraction of the power consumed to drive the process is about 47%, and about 10% of the synthesized biocrude must be consumed as internal back up.

Under these conditions a minimum selling price of the biocrude of 2.83 €/kg was estimated that is quite similar to that of biocrude obtained in non-solar processes [42].

4.3 Solar steam reforming

Steam reforming of natural gas is the most common method of producing commercial hydrogen. It combines steam and hydrocarbons that are reacting in a reformer at temperatures above 600°C to produce syngas. The syngas is mainly composed of CO and H_2. The syngas is then treated in order to improve the production yield and to achieve the required specifications and purity of the sold hydrogen. To provide the reactor with the required high temperature heat, a supplemental amount of the feedstock needs to be burned. An additional 40% of methane reacts with air to provide the process with the heat [43].

Hydrogen production via solar steam methane reforming (SMR), wherein concentrated solar radiation is the energy source of process heat, contributes to reduce CO_2 emissions due to the decrease in fossil fuel burning. Figure 18 shows a simplified flow chart of the solar reforming process.

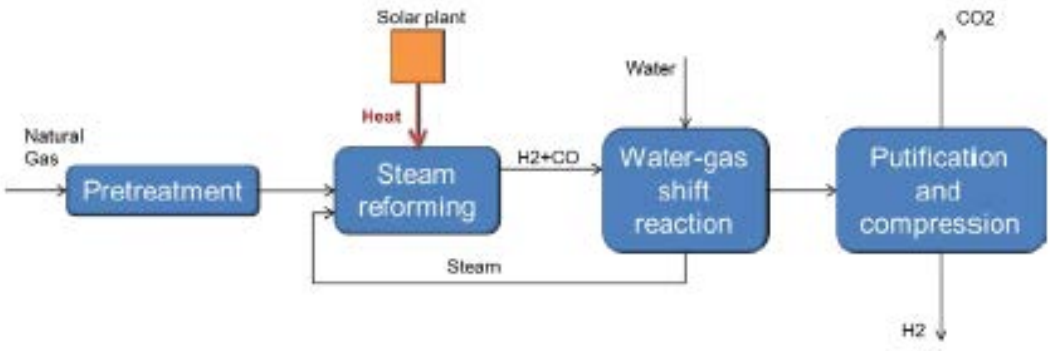

Figure 18: Flowsheet of the solar steam methane reforming (SMR).

The Aspen Plus main flowsheet of the solar SMR process shows several hierarchy blocks describing different process operating units of the process. Five units are considered:

- SR+WGS: Steam reforming and water gas shift Unit
- CO2CAP: CO2 Capture Unit
- CO2COMP: CO2 Compression Unit
- PSA: Pressure Swing Adsorption Unit
- SOLAR: Solar loop Unit

This process model unit of the steam reforming and WGS reactions contains four equilibrium reactors (REquil):

- Pre-reformer
- Steam Methane Reformer (SMR)
- High-temperature Water-Gas-Shift (HTS)
- Low-temperature Water-Gas-Shift (LTS)

The process has two main feed streams: natural gas (NG) and water (WATERIN). The natural gas is mixed with two recycling streams (PSAOFF and METHANE) before being further associated with preheated steam. The pressure of reactants is fixed at 27 bars. The steam is generated by using a heat recovery system. The feed water is pumped into the process. A pressure of 31 bars is calculated after considering the pressure drop in each heat exchanger. The feed water is preheated and then evaporated using the heat of the exothermic shift reaction, and the syngas is leaving the low temperature shift reactor. The steam produced at 210°C is fed later to the top of the high temperature water-gas shift reactor and reaching a temperature of 232°C. The last heating step occurs on top of the main reformer where the syngas is cooled from 900°C to 350°C. The steam is superheated until 800°C and flows with the gas mixture into the pre-reformer. Under those conditions, no heat is required for the activation of the highly endothermic cracking reaction in the pre-reformer. This heat recovery strategy allows saving almost 2496 kW, which usually is supposed to be supplied externally. The pre-preforming is assured at a range of 400-550°C [43]. For the Aspen simulation, the reactor temperature is chosen as 550°C in order to assure optimal preheating conditions for the main reformer.

Two CO_2 purification technologies have been investigated within the analysis of the solar steam reforming, namely the physical (Rectisol wash) and the chemical (MEA) separation. In order to compare which process is exergetically and energetically more suitable and more effective, a CO_2 recovery of 94% was fixed for both processes. Figure 19 shows the results of the exergy analysis of the steam reforming process for the two CO_2-separation technologies. The exergy efficiency of the solar steam methane reforming is defined as the ratio of the product exergy flow recovered in the hydrogen stream to the total exergy delivered into the system. The exergy efficiency is given by the following equation:

$$\eta_{exergy} = \frac{\dot{E}_{H2}}{\dot{E}_{NG} + \dot{E}_{elec} + \dot{E}_{Heat} + \dot{E}_{Cooling}} \quad (1)$$

The analysis shows that the chemical separation of CO_2 is the most efficient process based on the exergy efficiency, which was calculated to be at 67.53% according to Eq. 1.

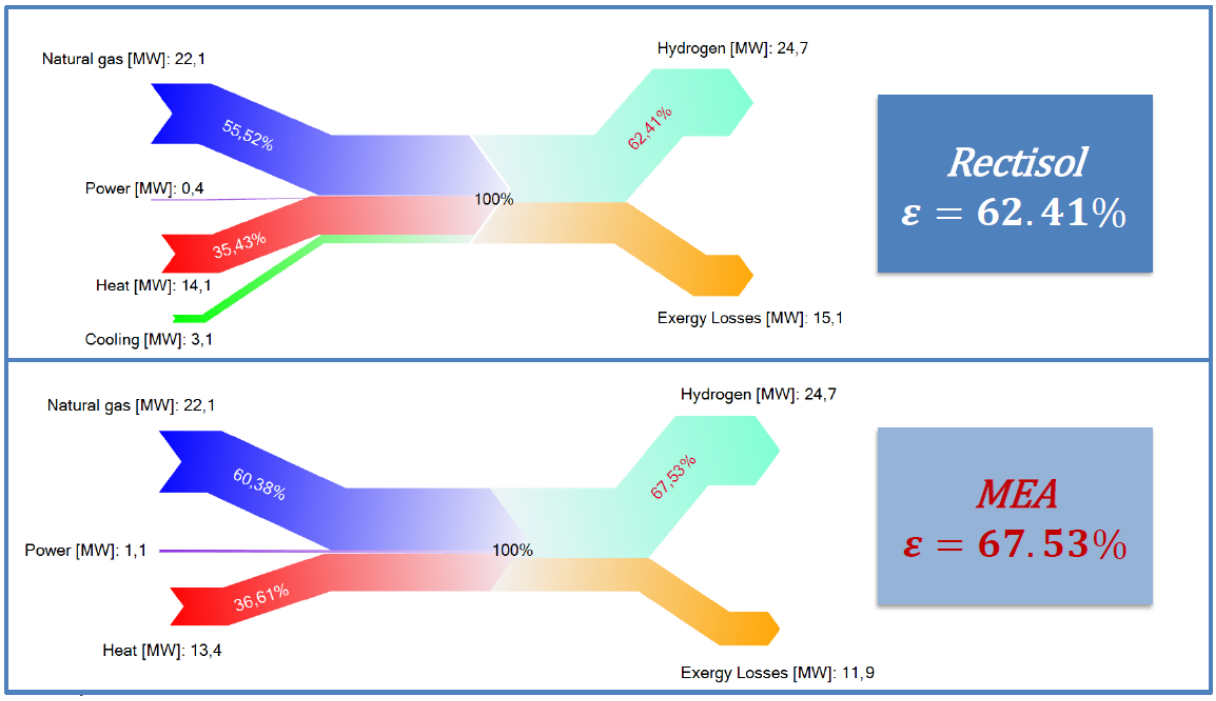

Figure 19: Exergy analysis of the solar steam reforming for both separation technologies.

The design of the CSP solar tower is generated by DLR's internally developed software HFLCAL. According to the latitude and the elevation of the site as well as the operating conditions of the receiver and the plant thermal duty, the layout of the concentrating solar tower and the heliostats field is devised. Table 5 shows the results of the design of the solar part of the plant.

Table 5: Design parameters of the solar part of the plant

Parameter	Value
Receiver inlet temperature [m²]	309
Receiver outlet temperature [°C]	920
Thermal duty of the receiver [°C]	25
Tower height [m]	60
Tower diameter [m]	16
Heliostat area [m²]	122
Number of heliostat	365

4.4 Solid Oxide Electrolysis

Since 1990, more than 40 international power-to-gas (P2G) pilot plants have been installed, producing hydrogen for grid balancing [44]. With P2G, excess electricity is converted into hydrogen by water electrolysis. This hydrogen can be stored in pressurized tanks and, when needed, reconverted into electricity with fuel cells or hydrogen combustion engines. Besides its use as an energy vector for electricity, hydrogen can serve as fuel for transport applications, as a raw material for the chemical industry, or for the synthesis of various hydrocarbon fuels such as methane. Additionally, a certain percentage of hydrogen could be directly fed into the gas distribution system; furthermore, there should be no limitations if hydrogen is previously converted to methane [44]-[45].

Current P2G projects commonly integrate alkaline or proton exchange membrane (PEM) electrolysers for hydrogen generation due to the maturity of this technology. However, the energy consumption of water electrolysis is still above 4.5 kWh_e/Nm^3 of hydrogen, and these plants as well require a second system to convert the hydrogen back to electricity [45]-[46]. These hydrogen-to-electricity systems usually are PEM fuel cells or internal engines [44]. High temperature steam electrolysis with solid oxide cells shows great advantages vis-à-vis conventional alkaline and PEM electrolysers [46]. These advantages stay on its high operational temperature range of 600–1000ºC. From a thermodynamic point of view, the water splitting reaction can be described by the Gibbs function,

$$\Delta G = \Delta H - T \cdot \Delta S \tag{2}$$

where ΔH is the overall energy needed, ΔG the electrical energy, and $T \cdot \Delta S$ the direct heat. As can be seen in Figure 20, electrical requirement decreases and heat energy demand increases with increasing temperature. Even though total energy demand increases, the decrease in electrical energy demand is more noticeable. Operation at high temperature can therefore decrease the electricity consumption and projects less generation cost. Cost reduction can be greater if the heat energy demand can be fulfilled by industrial waste heat [46]-[47].

From a kinetic point of view, high temperature helps to promote electrode activity and reduce cell overvoltage. It means that power density can be increased, reducing the size of the electrolyser for a given hydrogen production. On the other hand, lower cell overvoltage can translate to lower energy losses, thus a more electric-efficient process [48]. Additionally, solid oxide systems are able to work either as electrolyser (SOEC) or as fuel cell (SOFC), reducing the number of units and its auxiliary elements.

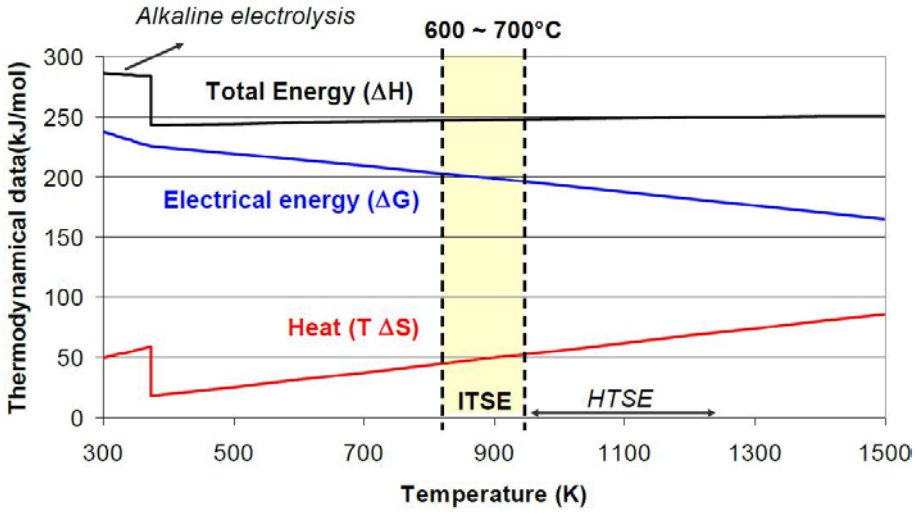

Figure 20: Free energy water splitting diagram. Temperature interval 600-700ºC would apply to Intermediate Temperature Steam Electrolysers (ITSE). High Temperature Steam Electrolysers (HTSE) require temperatures above 700ºC.

In the literature, several studies can be found on hydrogen production in hybrid plants, where SOEC systems are integrated into solar, biomass, or nuclear power plants [49]-[52]. In this work, a solar SOEC hybrid plant is designed as grid balancing system. The main goal of the proposed system is to reduce power demand fluctuations between high and low demand periods. Thus, the hybrid plant is analysed for the production of hydrogen during low demand periods using electricity taken from the grid, which results in flattening the demand curve. Additionally, based on these simulations, the ability of the plant to operate as an active grid balancing system is evaluated.

4.4.1 Coupling of a solid oxide cell unit and a linear Fresnel reflector field

In this scheme, a hybrid solar hydrogen plant composed of a concentrating solar thermal plant and a solid oxide system is implemented. The CSP system is only required for heat supply. Thus, based on its simplicity and the low cost of the components, a linear Fresnel reflector coupled to a thermal energy storage (TES) system lined with castable refractory was selected [53]-[54].

Annual yield analysis of the proposed hybrid plant will be carried out, in order to analyse the capability of the plant to produce hydrogen during night to increase the electricity demand. Thereby, the potential of the plant to flattening the electricity demand curve will be evaluated as function of the number of TES modules implemented in the solar plant. The results should demonstrate that the hybrid plant is able to produce enough hydrogen to feed a hydrogen bus refuelling station with a capacity of 20 metropolitan busses.

The hybrid solar-hydrogen plant analysed in the present study is composed of a solid oxide

unit and a LFR coupled with a thermal storage systems. The layout of the plant is presented in Figure 21. The upper section depicts the solar concentrating thermal system, which consists of several LFR collectors and a number of castable refractory TES modules. In the middle of the scheme, the electrolysis system is shown. Finally, the compression and storage system is visible at the bottom of the figure. In both scenarios, hydrogen is compressed up to 30 bar before it is delivered to the refuelling station or stored for later use in the fuel cell.

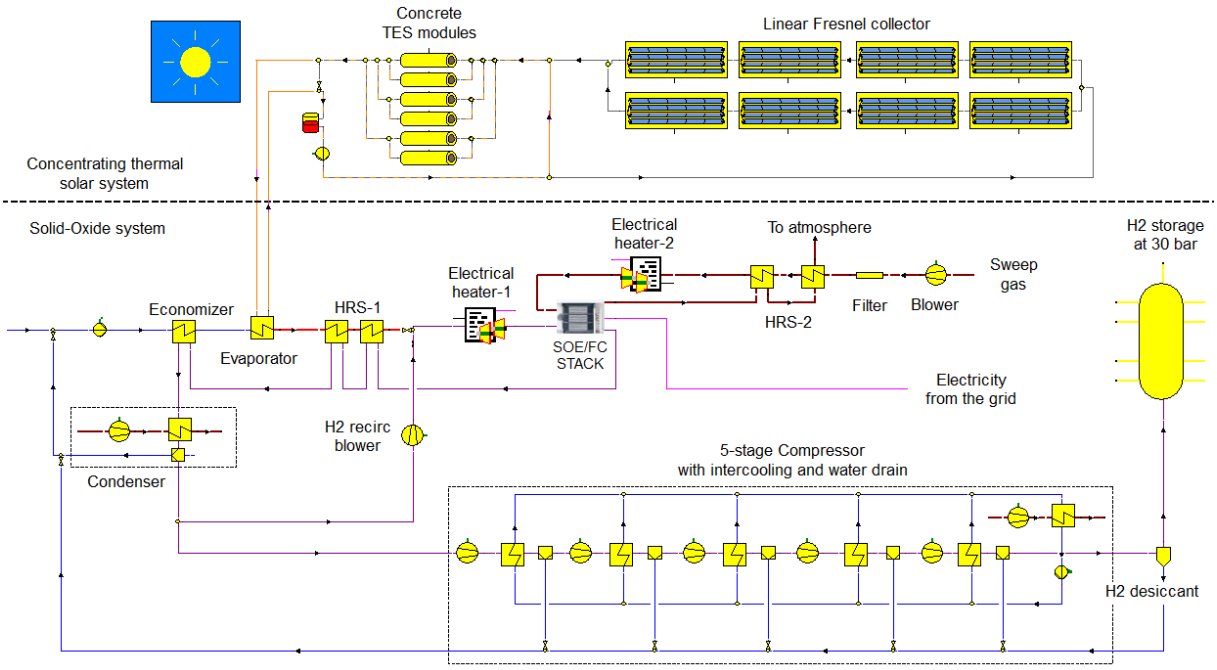

Figure 21: Scheme of the hybrid solar hydrogen plant with a Linear Fresnel collector field and a Solid Oxide Electrolyser.

Although LFR normally uses water as heat transfer fluid due to the characteristics of this system that include no requirements for power production from the solar plant, the temperature level (above 300 ºC), the displacement in time of collecting and delivering heat, and the requirement of maximum simplicity to reduce cost. Thermal oil was retained as heat transfer fluid avoiding the phase change transition at this temperature level. Eight Mirroxx LFR collectors, grouped in two parallel lines of four collectors in series, were implemented. The thermal storage system consists of few castable refractory TES modules of 10 m length and 4.84 m^2 cross section.

The electrolysis system comprises two units of 2.5 MW_e each. It consists of 38,400 cells with an active area of 80 cm^2. It is assumed that the electrolyser stack operates at 700ºC at the thermo-neutral voltage, which corresponds to a cell voltage of 1.281 V and a current density of 0.63 A/cm^2, with a steam conversion rate of 60 %, and a molar ratio between the anode and cathode of 1:1. Under these operational conditions, the overall energy efficiency of the electrolyser – defined as the ratio between the lower heating value (LHV) of the generated

hydrogen and the stack power needed to perform this task – is 97%. Furthermore, to prevent the degradation of the cathode, reducing conditions in the cathode chamber have been ensured with the recirculation of a fraction of hydrogen into the cathode feed steam, contributing to 10 vol% of hydrogen content.

4.4.2 Coupling of a Solid-Oxide cell unit and a DSG solar Tower

Direct steam generation (DSG) tower plants have shown to be able to deliver heat and electricity required for HTE. The system consists of the DSG solar tower, the HTE unit and the heat recovery system. The DSG solar tower system includes the tower, the solar receiver and the heliostat field, which reflects the incident solar radiation onto the receiver, as well as the thermal storage and the engine, which converts heat into mechanical work. An electrical generator, attached to the heat engine, generates electricity.

Steam is heated up in the receiver and absorbing the highly concentrated solar radiations reflected by the heliostats to convert it into thermal energy. Part of this thermal energy is generating electrical energy for the high temperature steam electrolyser. Another portion of the thermal energy is loading the thermal storage system. A third stream is used to heat the sweep gas required for the electrolyser. The heat recovery system aims at overheating the steam up to the operating temperature of the electrolyser. It consists of two heat exchangers (SUPERHX2, SUPERHX3). Figure 22 shows a simplified flow chart of the plant, which has been elaborated with Microsoft Visio, in order to achieve more clarity.

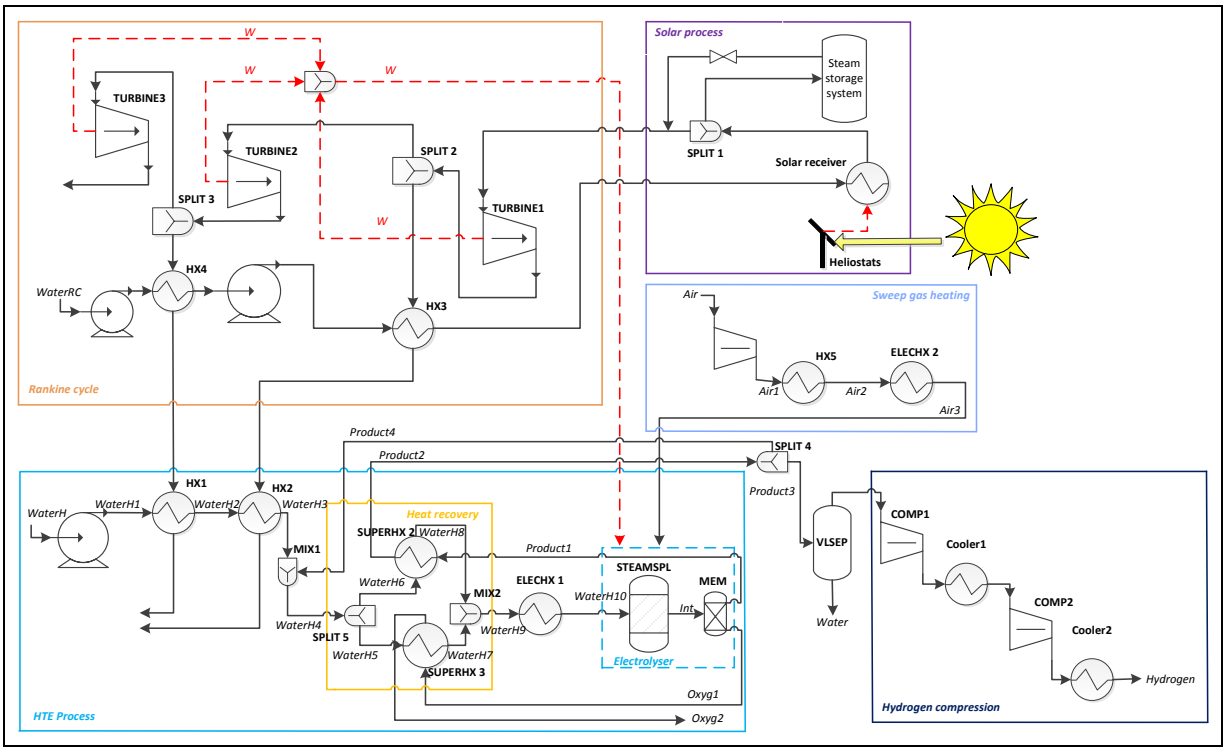

Figure 22: Flow sheet of HTE coupled with DSG solar tower.

For the simulation, a sweep gas to steam ratio of 1:1 was assumed. Table 6 shows the simulation results of the process units for 400 and 4000 kg/d hydrogen production.

Table 6: Simulation results of the main components for HTE coupled with DSG solar power plant.

Component	**Heat duty / power [MW]**	
	400 kg/d H_2	**4000 kg/d H_2**
ELECHX1	0.091	0.991
ELECHX2	0.091	0.991
SUPERHX2	0.097	0.896
SUPERHX3	0.097	0.896
HX1	0.017	0.167
HX2	0.599	5.987
HX5	0.007	0.068

The process efficiency – related to the thermo-electrical part of the process excluding the solar part – was then calculated according to the following equation:

$$\eta = \frac{\dot{m}_{H_2} LHV_{H_2}}{\dot{Q}_{receiver} + \sum \dot{W}} \quad (3)$$

With $Q_{receiver}$ being the solar heat feeding to the process and ΣW representing the sum of the power of the electrical heaters, pumps, etc., the process efficiency is calculated to be 18.6%.

The solar part of the process was dimensioned and optimised for the DSG solar tower plant. In this case, state-of-the-art storage is available for two hours, which makes difficult keeping hot the stack during day and night, independently of the external grid. For an annual average daily production of 400 kg hydrogen, the heliostat field consists of 146 heliostats with a reflective surface of 121.34 m² each. The total heliostat surface area is about 17,715 m².The tower has a height of 83 m and the solar receiver an aperture of 15.3 m². This results in an annual optical efficiency of 64.4%. For a plant producing 4000 kg/d hydrogen, the heliostat field consists of 1,836 heliostats with a reflective surface area of 121.34 m² each. The total heliostat surface is about 222,780 m². The tower has a height of 124 m and the solar receiver an aperture of 154 m². It results in an annual optical efficiency of 51.4 %.

If such hydrogen production capacity is required every day of the year, the heliostat field has to be laid out at the design point on the 21st of December at noon. In this case, more heliostats are needed as shown Table 7.

Table 7: Layout of the heliostat filed for coupling with DSG solar tower plant.

Component	**400 kg/d H_2**		**4000 kg/d H_2**	
Annual average receiver power [MW]	11		107	
Design point	21.03. at noon	21.12. at noon	21.03. at noon	21.12 at noon
Tower height [m]	83	83	151	151
Number of heliostat	146	184	1661	2108
Receiver aperture [m²]	15.3	15.3	154	154
Annual optical efficiency [%]	64.4	62.9	56.2	52.9

4.4.3 Coupling of a Solid-Oxide cell unit and a Molten Salt solar Tower

The molten salt solar tower technology has been investigated as a single energy source regarding electricity and heat generation. The analysis has shown that this technology is able to provide the electrolyser with the required energy in order to run the electrolysis process. The system consists of the molten salt tower, the HTE unit and the heat recovery system. The molten salt tower system includes the tower, the solar receiver and the heliostat field, which reflects the incident solar radiation onto the receiver, as well as the thermal storage and the engine, which converts heat into mechanical work. An electrical generator, attached to the heat engine, generates electricity.

Molten salts are heated up to temperatures of about 565°C in the receiver and absorbing the highly concentrated solar radiations reflected by the heliostats to convert it into thermal energy. A part of this thermal energy is used in the boiler to generate steam, which, in turn, is transported to a steam turbine. The steam expands in the turbine producing mechanical work, which is then converted through a generator into electrical energy for the high temperature steam electrolyser. Part of this steam is evaporating the water and heating the steam (HX1, HX2) required for the stack, which has another quality than the steam used in the turbine. Another portion of the thermal energy is loading the thermal storage system in order to resolve the time-dependent performance of the solar collector field as well as the solar transients and fluctuations, and thus to ensure constant feed for the electrolyser. A third stream is used to heat the sweep gas required for the electrolyser in HX5. The heat recovery system aims to overheat the steam up to the operating temperature of the electrolyser. It consists of two heat exchangers (SUPERHX2, SUPERHX3).

Figure 23 shows a simplified flowchart of the plant, which has been elaborated with Microsoft Visio.

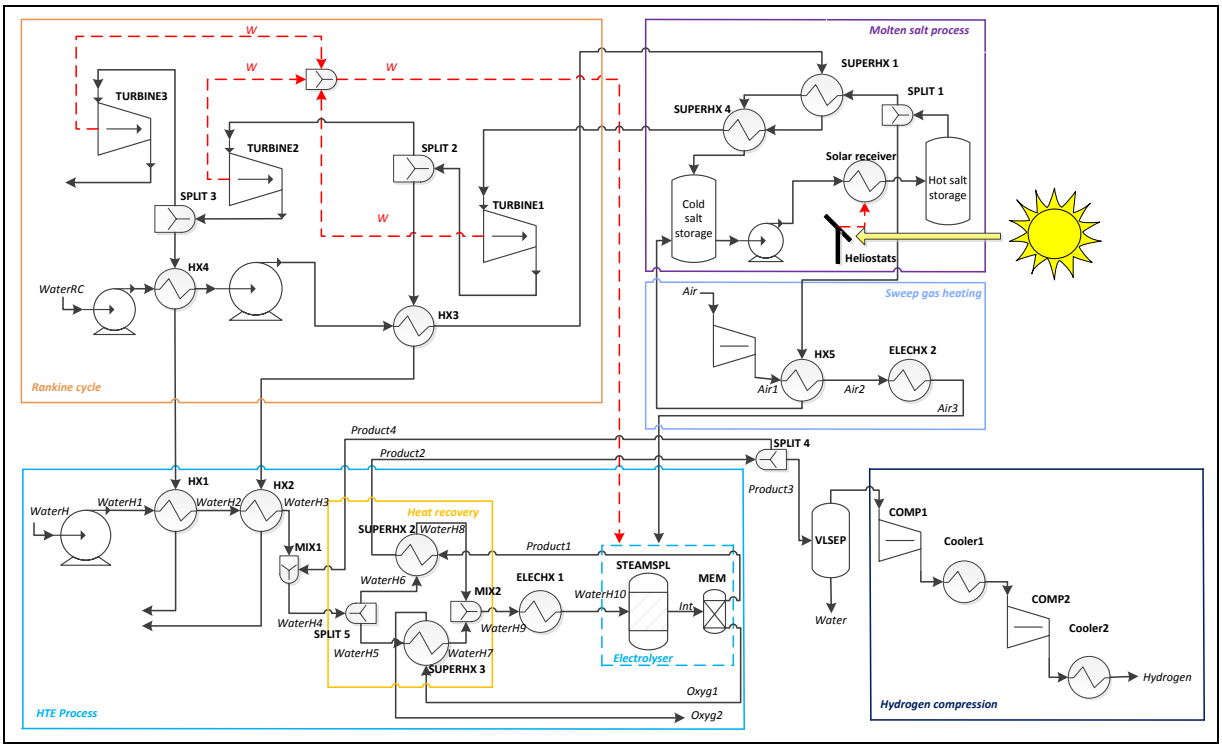

Figure 23: Flow sheet of the HTE process coupled to a molten salt solar tower plant.

For the simulation, a sweep gas to steam ratio of 1:1 was assumed. Table 8 shows the simulation results of the process units for 400 and 4000 kg/d hydrogen production.

Table 8: Simulation results of the main components for HTE coupled with molten salt plant.

Component	**Heat duty power [MW]**	
	400 kg/d H_2	**4000 kg/d H_2**
SUPERHX1	2.221	23.11
ELECHX1	0.089	0.94
ELECHX2	0.092	0.88
SUPERHX2	0.097	0.98
SUPERHX3	0.097	0.98
HX1	0.017	0.18
HX2	0.598	6.11
HX5	0.019	0.25

The process efficiency – related to the thermo-electrical part of the process excluding the solar part – was then calculated according to the following equation:

$$\eta = \frac{\dot{m}_{H_2} \, LHV_{H_2}}{\dot{Q}_{receiver} + \sum \dot{W}} \tag{3}$$

With $Q_{receiver}$ being the solar heat feeding to the process and ΣW representing the sum of the power of the electrical heaters, pumps, etc.

The overall efficiency considering also the heliostat field optical efficiency will be calculated for selected locations because the heliostat field efficiency depends on the solar input data and thus on the location of the plant. A process efficiency of about 14% is obtained. The solar part of the process was dimensioned and optimised for the MS solar tower plant. In this case, storage is implemented working 16 hours in order to keep hot the high temperature electrolyser night and day. With the integration of the storage system in a plant having an annual average daily production of 400 kg/d hydrogen, the heliostat field consists of 198 heliostats with a reflective surface area of 121.34 m² each. The total heliostat surface is about 24,025 m². The tower has a height of 125 m and the solar receiver an aperture of 24 m². It results in an annual average solar efficiency of 59.2%.

In the case of a plant producing 4000 kg/d hydrogen (annual average daily production), the resulting heliostat field has 2,102 heliostats with a reflective surface of 121.34 m² each. The total heliostat surface area is about 255,056 m². The tower has a height of 200 m and the solar receiver an aperture of 192 m². It results in an annual average solar efficiency of 56.8%.

If this hydrogen production capacity is required each day of the year, the heliostat field has to be laid out at the design point on 21st of December at noon. In this case, more heliostats are needed, as shown in Table 9.

Table 9: Layout of the heliostat field for coupling with molten salt solar tower plant

Component	**400 kg/d H_2**		**4000 kg/d H_2**	
Annual average receiver power [MW]	14		138	
Design point	21.03 at noon	21.12 at noon	21.03 at noon	21.12 at noon
Tower height [m]	125	125	200	200
Number of heliostat	198	245	2102	2563
Receiver aperture [m²]	24.15	24.15	192.85	192.85
Annual average solar efficiency [%]	59.2	58.9	56.8	55.5

4.5 Molten Carbonate Electrolysis

In order to reduce the temperature gap with current solar thermal fluids, development of electrolysis processes within the 500-600°C range would be a desirable option. In this context, molten salts could be seen as an ideal medium to lower process temperatures with respect to solid oxide electrolysers since overall ionic conductivity and transport numbers of liquid salts are usually higher than solid-type electrolytes. Recently, alkali molten carbonate salts have gained a return of attention as versatile electrolytes for conducting electrochemical conversion processes of mineral ores and CO_2 gas at moderate temperatures [55]-[56].

In this context, molten carbonate electrolysis (MCE) to produce hydrogen from water is another process mentioned recently in literature [57], although no systematic studies on this process have been conducted so far. Only very recently, the feasibility of a MCE process for hydrogen production has been demonstrated in laboratory scale experiments in the 600-675°C range using a molten carbonate fuel cell (MCFC) operated in a reverse (electrolysis) mode [58]. The present analysis is focused onto Ni-based MCFC electrodes since they behave as efficient bi-functional electro-catalysts, although long-term and more detailed studies are warranted, especially to evaluate the electrolysis corrosion effects on MCFC electrodes and thus to demonstrate the feasibility of a reversible MCFC concept.

The overall electrolysis reactions can be written as:

$$H_2O + CO_2 + 2e^- = H_2 + CO_3^{2-} \quad (4)$$

$$CO_3^{2-} = CO_2 + ½\ O_2 + 2e^- \quad (5)$$

Several peculiar aspects of a water MCE process are noteworthy. Firstly, it may be observed that the anode reaction does not produce pure oxygen, but a CO_2:O_2 gas mixture, which is ideal for use in oxy-combustion processes. In fact, the anodic off-gas is composed of a 2:1 CO_2:O_2 mixture that is comparable in terms of adiabatic temperature to an air stoichiometric combustion [59]. Secondly, since the cathode reaction needs a CO_2 source, a CO_2 closed-loop system with CO_2 capture could be easily realised by an integrated electrolysis and oxy-combustion process. In fact, part of the post-combustion CO_2 could be re-injected to the cathode, whereas the excess CO_2 could be easily captured or used.

In the first proposed scheme, a Linear Fresnel system like the one used in the previous section for SOEC is modified to extract some heat from the storage to produce the steam needed at a molten carbonate electrolyser (Figure 24).

In the second proposed scheme shown in Figure 25, a typical molten salt CRS system is modified to extract some heat from the low temperature tank to produce the steam needed at a molten carbonate electrolyser (MCE).

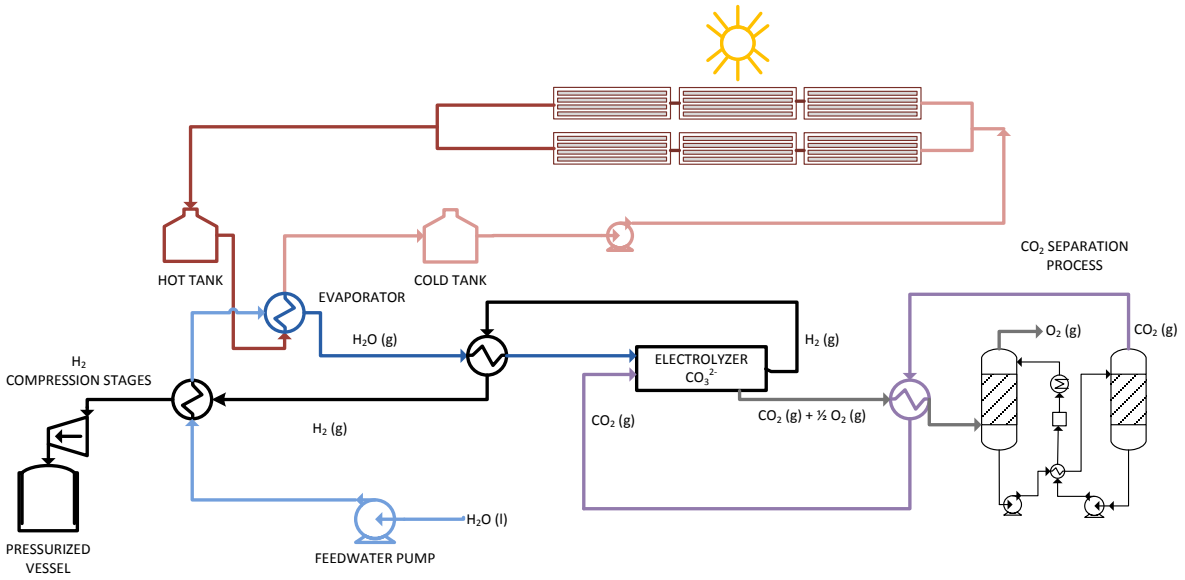

Figure 24: Scheme of the solar-hydrogen plant with a linear Fresnel reflector field and a molten carbonate electrolyser (MCE).

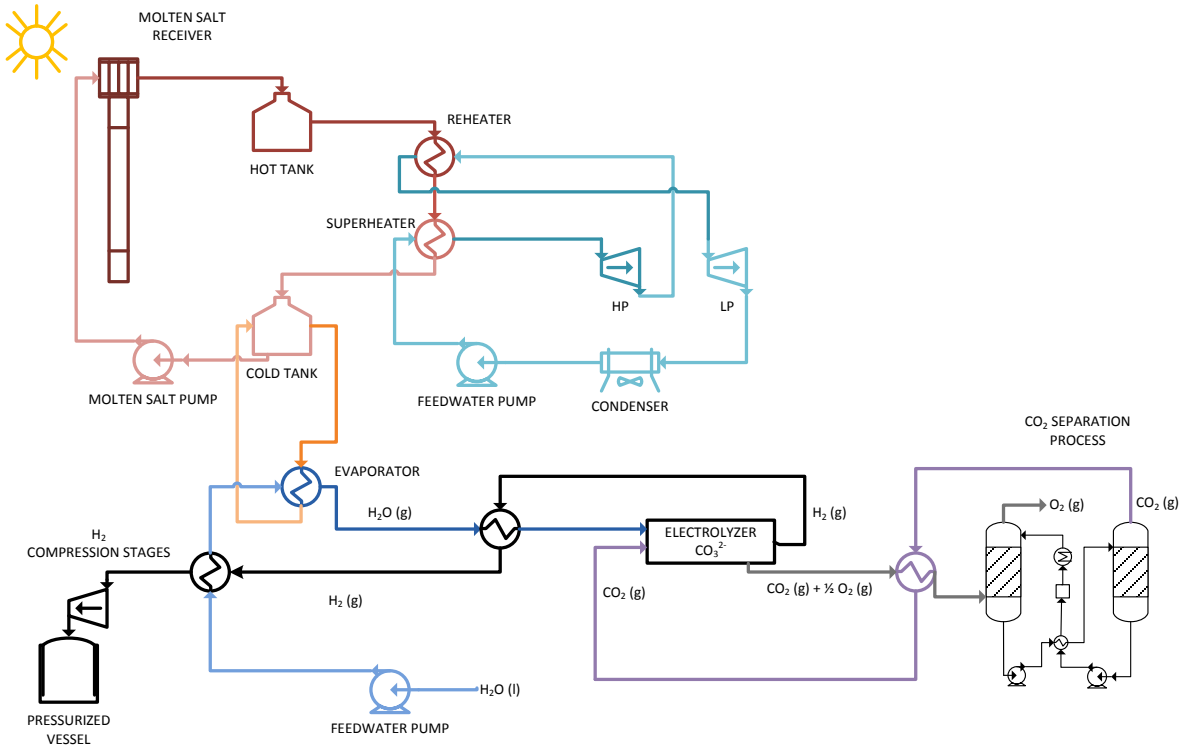

Figure 25: Scheme of the solar-hydrogen hybrid plant with a central receiver system (CRS) with molten salts and a molten carbonate electrolyser (MCE).

5. Process screening of thermochemical cycles

A screening of thermochemical cycles was performed. This comprises different reactions, which take place in a range of temperatures between 500 and 1500ºC. The selection process has to take into account the availability and cost of raw materials in the market for each reactant or product involved in these reactions. The first phase of this study included different industrial processes for producing commodities. In this specific temperature range, there are not many reversible reactions, but among them, there are some systems based on CO_2/CO and H_2/H_2O.

5.1 CO_2/CO systems

Overall, these reactions are participating in CO_2 capture or recycling systems, thus allowing valorising CO_2, which can be reduced by means of the following reaction:

$$CO_{2\,(g)} \rightarrow CO_{\,(g)} + ½\ O_{2\,(g)} \quad (6)$$

The reaction takes place at very high temperature in the range of 2,000–2,400ºC. Therefore, researchers are seeking new reactants that can easily be reduced at lower temperature. The products from this kind of reactions can be useful in the Fischer-Tropsch reaction, which is known for producing hydrocarbons or storing thermal energy by means of the same reaction.

There are also other methods to reduce CO_2 in the atmosphere by means of fixing the CO_2 in a solid. This process in known as sequestration of CO_2. However, this reaction cannot be considered a redox reaction. Enthalpies of all reactions investigated are referred to the standard enthalpy of reaction ΔH_r^o at 298.15 K and atmospheric pressure. Besides, none of those reactions will increase significantly the work pressure due to running at chemical equilibrium conditions. The only energetic variation will be that of thermal energy. Table 10 shows various reactions, equilibrium temperatures and enthalpies related to the CO_2/CO systems investigated.

Table 10: Summary of CO_2/CO systems investigated.

Reaction	T [ºC]	ΔH_r^o [kJ/mol]
$CO\ (g) + H_2O\ (g) \leftrightarrow CO_2\ (g) + H_2\ (g)$	350-500	-41
$3\ Fe_2O_3\ (s) + CO\ (g) \leftrightarrow 2\ Fe_2O_4\ (s) + CO_2\ (g)$	200-700	-47
$Fe_3O_4\ (s) + CO\ (g) \leftrightarrow 3\ FeO\ (s) + CO_2\ (g)$	850	-34
$ZnO\ (s) + CO\ (g) \leftrightarrow Zn\ (g) + CO_2\ (g)$	910-1,223	67.5
$Al_2O_3\ (s) + 3\ CO\ (g) \leftrightarrow 2\ Al\ (l) + 3\ CO_2\ (g)$	1,000	1,606.6
$PbO\ (s) + CO\ (g) \leftrightarrow Pb\ (l) + CO_2\ (g)$	350-925	-65.7
$CeO_{2-x} + x\ CO_2 \leftrightarrow CeO_2 + x\ CO$	827-1,640	480-384

5.2 H_2/H_2O systems

Hydrogen gas is a very reductive compound provoking highly exothermic reactions, which have properties of explosive gas in contact with different elements (Table 11). However, hydrogen can take place in reactions at odd working conditions thanks to its reducing properties (it is more reductive than C and CO) [60]-[61].

Table 11: Summary of H_2/H_2O systems investigated

Reactions	T[ºC]	ΔH_r^o [kJ/mol]
Fe_3O_4 (s) + H_2 (g) ↔ 3 FeO (s) + H_2O(g)	570	55
ZnO (s) + H_2 (g) ↔ Zn (g) + H_2O(g)	700-900	108
Al_2O_3 (s) + 3 H_2 (g) ↔ 2 Al (l) + 3 H_2O (g)	1,000	1,711.1
CeO_{2-x} + x H_2O ↔ CeO_2 + x H_2	827-1,640	480-384

Enthalpies of all reactions investigated are referred to the standard enthalpy of reaction ΔH_r^o at 298.15 K and atmospheric pressure. Besides, none of those reactions will increase significantly the work pressure due to running at chemical equilibrium conditions. The only energetic variation will be that of thermal energy.

If the reactions are considered from the point of view of metal oxidation by means of water, in every case the reaction mechanism is as follows:

$$H_2O_{(g)} \leftrightarrow H_{2\,(g)} + ½\ O_{2\,(g)} \qquad (7)$$

In the presence of material that can easily be oxidized (Zn, Al or Fe), higher reaction temperature and higher reaction velocity move the reaction (7) towards the products and re-oxides the metal.

5.3 Perovskite cycle

Pervoskite cycles have also been explored for the solar production of CO and H_2. In perovskite structures, the elements are organised as an A cation and a B cation plus the oxygen anion.

Since cations can easily be replaced by similar elements, the compounds present a wide range of possible chemical behaviours while keeping a similar structure. Similarly, perovskites are mostly immune against some problems encountered by catalysts and other thermochemical storage (TCS) materials exposed to high temperatures, such as sintering and crushing. Apart from the unaffected perovskite structure, the porosity for oxygen transport eases the chemical

reaction for the solar production of H_2. Furthermore, since these structures proposed are made of common and available materials that can be obtained at reduced costs, perovskite cycles constitute an interesting route to be further explored. Table 12 shows some perovskite compositions currently being studied [62].

Table 12: Summary of perovskites cycles investigated

Structure	T_r [ºC]
$La_{1-x}Sr_xMn_{1-y}Al_yO_3$	800-1,320
$La_{1-x}Sr_xMnO_{3-\partial}$	800-1,000
$La_{1-x}Sr_xCo_{1-y}Fe_yO3_{3-\partial}$	300-1,000
$CaTi_{1-x}Fe_xO_3$	1,000-1,360
$NaMgF_3$	778

5.4 Hercynite cycle

Another reaction, which allows water splitting at lower temperatures than 1000ºC, is the one based on aluminium spinel structures. Table 13 below shows the reaction proposed [63].

Table 13: Hercynite cycle proposed

Structure	T_r(ºC)
$CoAl_2O_4 + 2FeAl_2O_4 + H_2O \leftrightarrow$ $CoFe_2O_4 + 3Al_2O_3 + H_2$ (g)	940-1,360

5.5 Other cycle

There is an additional chemical reaction, which does not fit as thermochemical storage system to the cycles considered so far. Table 14 shows the reaction of the copper-chlorine cycle [64].

Enthalpies of all reactions investigated are referred to the standard enthalpy of reaction ΔH_r^o at 298.15 K and atmospheric pressure. Besides, none of those reactions will increase significantly the work pressure due to running at chemical equilibrium conditions. The only energetic variation will be that of thermal energy.

Table 14: Copper chlorine cycle proposed

Reactions	T[ºC]	ΔH_r^o [kJ/mol]
Cu (s) + HCl (g) ↔ CuCl (s) + 1/2 H_2 (g)	450	-55.5

In principle, this reaction has not been analysed deeply because it is not considered as interesting as the reactions discussed above. In any case, a study will be performed under specific criterions to find out if this reaction is suitable for thermochemical storage systems.

6. Summary and Outlook

The main goal of this milestone was to define to the most suitable solar hydrogen production processes and to describe their integration with the solar energy source. The investigation of different CSP technologies was carried out by taking into account their ability to provide the processes with the required energy demand, which can be high temperature heat or/and electricity. In addition to that, a screening of different thermochemical cycles for water splitting was performed in order to identify the most suitable processes, which can be coupled to CSP technologies. The possibility of coupling with CSP was also considered for some examples of chemical conversion processes, such as methane steam reforming and hydrothermal conversion of microalgae to biocrude oil.

Several CSP technologies were analysed and the most promising ones were identified. Table 15 summarizes the energy conversion technologies with HTF and characteristic temperature range, which have been selected for coupling to the solar hydrogen production processes.

Table 15: Summary of CSP technologies investigated for integration with H_2 production processes.

Technology	Heat transfer fluid	Temperature [°C]
Air-cooled solar tower	Air	750
Molten salt solar tower	Molten salt	565
DSG tower	Water	550
Parabolic through	Thermal mineral oil	150-400
Linear Fresnel	Thermal mineral oil	150-400

The solar tower technology with air as heat transfer fluid (HTF) is able to provide chemical heat and/or electricity. A storage system for transient operation conditions is implemented. As this solar tower concept is working with hot air as HTF and as the electrolyser is running with hot air as sweep gas, a part of the solar-produced hot air coming from the tower can be used in high temperature electrolysis (HTE). This feature is a big advantage for this technology, especially regarding its coupling to the HTE process. The solar tower technology working with molten salt (MS) as fluid leads to a higher annual capacity due the long-term thermal storage system, which has been integrated and already demonstrated in these plants. The direct steam generation (DSG) solar tower can provide heat and electricity. Using water as the heat transfer medium has the advantage of being low cost, and it is neither flammable nor harmful to the environment.

Solar fuels can be produced via direct or indirect processes using concentrated solar energy. Table 16 shows the solar hydrogen production processes that will be considered for further analysis with the corresponding thermodynamic specification, mainly temperature and pressure.

Table 16: Summary of the hydrogen production processes investigated.

Process	**Temperature [°C]**	**Pressure [bar]**
Solid-oxide steam electrolysis	750	1
Molten-carbonate electrolysis	550	1
Steam reforming	900	28
Thermochemical water splitting	800-1,500	1
Solar MS-heated hydrothermal liquefaction of microalgae	410	1
Low temperature MS-heated steam reforming	450-550	10

The procedure of the system analysis consists of elaborating flowsheets of solar hydrogen production processes coupled to the energy conversion technology, the simulation of the processes and the economic analysis. The capacity of the scale-up plants have been defined at hydrogen production rate of 400 kg/day and 4000 kg/day, which correspond to a hydrogen refuelling station scenario and an industrial application, respectively. The flow-sheeting aims to the identification of the most suitable coupling scheme of the chemical processes to the CSP technology. After that, the simulation of the overall process is being carried out to calculate energy and mass balances, to calculate the solar-to-hydrogen efficiency of the processes and to provide the necessary information for the component sizing. Based on the results of the simulation and the component sizing, the economic analysis will be performed in the upcoming months.

The screening of the different thermochemical cycles of water splitting is still going on and a pre-selection of the most promising processes was made. Figure 26 shows an overview on the screening of the thermochemical cycles considered.

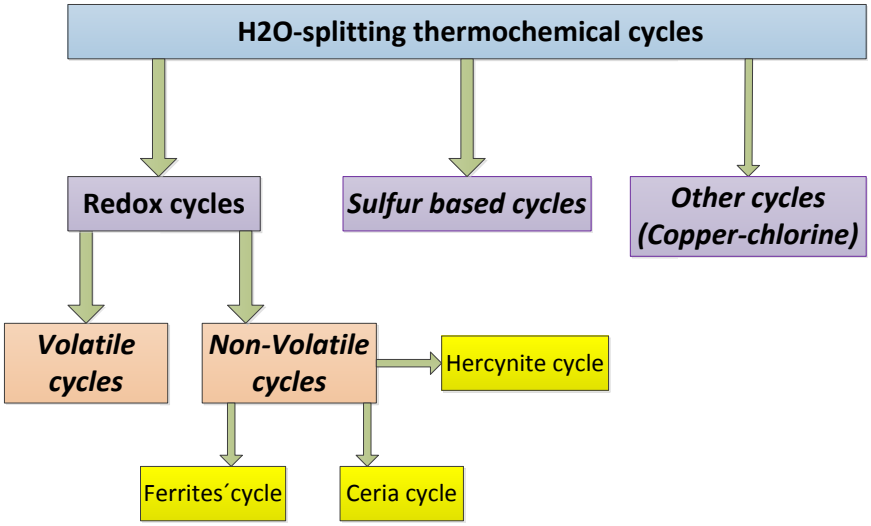

Figure 26: Screening of thermochemical cycles

It was decided by the WP9 consortium to consider the Hercynite, ceria and ferrite cycles for further analysis. The overall system analysis, which includes flow sheeting, simulation and economic analysis, will be carried out in the upcoming months.

7. List of abbreviations

ABENGOA	Abengoa Solar New Technologies SA, Spain
BMC	Bare Module Cost
BoP	Balance of Plant
CAPEX	Capital Expenses
CIEMAT	Centro de Investigaciones Energéticas, Medioambientales y Tecnológicas, Spain
CNRS	Centre National de la Recherche Scientifique, France
CRS	Central Receiver System
CSP	Concentrating Solar Power
CST	Concentrating Solar Thermal
DLR	Deutsches Zentrum für Luft- und Raumfahrt (German Aerospace Centre), Cologne, Germany
DMS	Direct Molten Salt
DSG	Direct Steam Generation
ENEA	Italian National Agency for New Technologies, Energy and the Sustainable Economic Development
GEF	Global Environment Facility
HTF	Heat Transfer Fluid
HTL	Hydro-Thermal Liquefaction process
HTSE	High Temperature Steam Electrolysis
HX	Heat Exchanger
IMDEA	Instituto Madrileño de Estudios Avanzados, Mósteles, Spain
ISCCS	Integrated Solar Combined Cycle System
ITSE	Intermediate Temperature Steam Elecrolysis
LFR	Linear Fresnel Reflector
MCE	Molten Carbonate Electrolysis
MEA	Mono Ethanol Amine
MENA	Middle East North Africa region
MCFC	Molten Carbonate Fuel Cell
MFSP	Minimum Fuel-Selling Price
MS	Molten Salt

NG	Natural Gas
NPV	Net Present Value
O&M	Operation and Maintenance
OPEX	Operation Expenses
P2G	Power To Gas
PCM	Phase Change Media
PEM	Proton Exchange Membrane
PSA	Plataforma Solar de Almería
PSI	Paul Scherrer Institute, Switzerland
PTC	Parabolic Trough Collector
SEGS	Solar Electricity Generating Systems
SMR	Steam Methane Reforming
SOE	Solid Oxide Electrolysis
SOEC	Solid Oxide Electrolyser Cell
SOFC	Solid Oxide Fuel Cell
SR	Solar Reforming
STE	Solar Thermal Electricity
TCS	Thermochemical Storage
TES	Thermal Energy Storage
UNIPA	Università degli Studi di Palermo, Italy
US	United States of America
WGS	Water Gas Shift

8. References

[1] J.E. Miller, A. Ambrosini, E.N. Coker, M.D. Allendorf, A.H. McDaniel. *Advancing oxide materials for thermochemical production of solar fuels.* Energy Procedia, 2014, 49, 2019–2026.

[2] G. Flamant, S. Abanades. *Thermochemical hydrogen production from a two-step solar-driven water-splitting cycle based on cerium oxides*. Solar Energy, 2006, 80, 1611–1623.

[3] M. Roeb, N. Gathmann. M. Neises, C. Sattler, R. Pitz-Paal. *Thermodynamic analysis of two-step solar water splitting with mixed iron oxides*. International Journal of Energy Research, 2009, 33, 893–902.

[4] I.E. O'Brien. *Thermodynamic Considerations for Thermal Water Splitting Processes and High Temperature Electrolysis*. Conference paper ASME 2008, USA.

[5] G. Towler, R. Sinnot. *Chemical Engineering Design: Principles, Practice and Economics of Plant and Process Design*. New York, Butterworth-Heinemann Publisher. 2007.

[6] M.S. Peters, K.D. Timmerhaus. *Plant Design and Economics for Chemical Engineers. Boston*. McGraw-Hill Publisher, 2004.

[7] L. Bertuccioli et al. *Development of Water Electrolysis in the European Union*. FCH-JU final report 2014.

[8] D. Barlev, R. Vidu, P. Stroeve. *Innovation in concentrated solar power*. Solar Energy Materials and Solar Cells, 2011, 95, 2703–2725.

[9] M. Romero, A. Steinfeld. *Concentrating Solar Thermal Power and Thermochemical Fuels*. Energy and Environmental Science, 2012, 5, 9234-9245.

[10] R. Pitz-Paal, J. Dersch, B. Milow. E*COSTAR: European Concentrated Solar Thermal Road-Mapping*, 2005.

[11] European Academies Science Advisory Council (EASAC). *Concentrating Solar Power: its potential contribution to a sustainable energy future*, 2011.

[12] S. Zunft et al. *Jülich Solar Power Tower – Experimental evaluation of the storage subsystem and performance calculations*. 16th SolarPACES International Symposium 2010, Perpignan, France.

[13] R.O. Gonzalez-Aguilar et al. *PS 10, construction of a 11MW solar thermal tower plant in Seville Spain*. SolarPACES 2006, Granada, Spain.

[14] C.E. Tyner and J.E. Pacheco, *Solar's power plant architecture*. SolarPACES 2006, Granada, Spain.

[15] T. Bauer et al. *Overview of Molten Salt Storage Systems and Material Development for Solar Thermal Power Plants.* World Renewable Energy Forum, USA, 2012.

[16] R.I. Dunn, P.J. Hearps and M.N. Wright. *Molten-Salt Power Towers: newly commercial concentrating solar energy*. IEEE 2012.

[17] H. Price, E. Luepfert, D. Kearney, E. Zarza, G. Cohen, R. Gee, R. Mahoney. *Advances in Parabolic Trough Solar Power Technology*, Int. J. Solar Energy Eng., 2002, 124, 109–125.

[18] Fernandez-Garcia A., Zarza E., Valenzuela L., Perez M. *Parabolic-trough solar collectors and their applications*. Renewable and Sustainable Energy Reviews, 2010, 14, 1695–1721.

[19] A. Rabl. *Active Solar Collectors and Their Applications*. New York, Oxford University Press, 1985: pp. 59–66. ISBN: 0-19-503546-1.

[20] M. Eck, E. Zarza, M. Eickhoff, J. Rheinländer, L. Valenzuela. *Applied research concerning the direct steam generation in parabolic troughs*. Solar Energy, 2003, 74, 341–351.

[21] D.W. Kearney, G.E. Cohen. (1997) *Current experiences with the SEGS parabolic trough plants*. In: Proc. 8th International Symposium on Solar Thermal Concentrating Technologies. Vol. 1. Cologne, Germany, 1996. Becker, M.; Böhmer, M. eds. Heidelberg, Alemania, C.F. Müller, 1997: pp. 217–224.

[22] O. Goebel. *Shams One 100 MW CSP Plant in Abu Dhabi*. Proc. SolarPACES 2009 (CD). Ref. manuscript: 15523; Berlin, Germany; 15-18 September 2009. Ed. DLR, Stuttgart, Germany. ISBN 978-3-00-028755-8.

[23] M. Romero. *Solar Thermal Power Plants*. In: Report on research and development of energy technologies. Edited by IUPAP working group on energy; October 6, 2004: pp. 96–108.

[24] M. Horn, H. Führing, J. Rheinländer. *Economic analysis of integrated solar combined cycle power plants. A sample case: The economic feasibility of an ISCCS power plant in Egypt*. Energy, 2004, 29, 935–1011.

[25] S. Relloso, E. Delgado. *Experience with molten salt thermal storage in a commercial parabolic trough plant. Andasol-1 commissioning and operation*. Proc. SolarPACES 2009 (CD). Ref. manuscript: 11396; Berlin, Germany; 15-18 September 2009. Ed. DLR, Stuttgart, Germany. ISBN 978-3-00-028755-8.

[26] M. Falchetta, D. Mazzei, T. Crescenzi, L. Merlo. *Design of the Archimede 5 MW molten salt parabolic trough solar plant*. Proc. SolarPACES 2009 (CD). Ref. manuscript: 11608; Berlin, Germany; 15-18 September 2009. Ed. DLR, Stuttgart, Germany. ISBN 978-3-00-028755-8.

[27] D. Laing, W.-D. Steinmann, R. Tamme, C. Richter. *Solid Media Thermal Storage for Parabolic Trough Power Plants*, Solar Energy, 2006, 80(10), 1283–1289.

[28] D. Laing, C. Bahl, T. Bauer, D. Lehmann, W.D. Steinmann. *Thermal energy storage for direct steam generation*. Proc. SolarPACES 2009 (CD). Ref. manuscript: 12055; Berlin, Germany; 15-18 September 2009. Ed. DLR, Stuttgart, Germany. ISBN 978-3-00-028755-8.

[29] M. Liu, W. Saman, F. Bruno. *Review on storage materials and thermal performance enhancement techniques for high temperature phase change thermal storage systems*, Renewable and Sustainable Energy Reviews, 2012, 16, 4, 2118–2132.

[30] E. Zarza, L. Valenzuela, J. Leon, K. Hennecke, M. Eck, H.D. Weyers, M. Eickhoff. *Direct steam generation in parabolic troughs: Final results and conclusions of the DISS project.* Energy, 2004, 29(5-6), 635–644.

[31] D. Mills, *Advances in solar thermal electricity technology*. Solar Energy, 2001, 76, 19-31.

[32] S.A. Kalogirou. *Solar thermal collectors and applications.* Progress in Energy and Combustion Science, 2004, 30, 231–328.

[33] A.T. Kearney. *Solar Thermal Electricity 2025, in STE industry roadmap for the European Solar Thermal Electricity Association* (ESTELA), 2010.

[34] M. Berger, A. Häberle, J. Louw, T. Schwind, C. Zhaler. *Mirroxx Fresnel process heat collectors for industrial applications and solar cooling*. SolarPACES 2009, Berlin, Germany.

[35] FRENELL (2016) White Paper "Solar Power on Demand. Least Cost Opportunity for Sun-rich Countries. Available at http://www.frenell.de/news/#N1

[36] A. Gioconia et al. *Multi-fuelled Solar Steam Reforming for Pure Hydrogen Production Using Solar Salts as Heat Transfer Fluid*. Energy Procedia, 2015, 69, 1750–1758.

[37] European project MATS – Multipurpose Applications by Thermodynamic Solar, Contract N° 268219.

[38] P.J. Valdez, V.J. Tocco, P.E. Savage. *A general kinetic model for the hydrothermal liquefaction of microalgae*. Bioresour. Technol., 2014, 163, 123–127.

[39] R. Turton, R. C. Bailie, W. B. Whiting, J. A. Shaeiwitz, and D. Bhattacharyya. Analysis, Synthesis, and Design of Chemical Processes. Pearson Education, Inc., 2013.

[40] M.S. Peters, K.D. Timmerhaus, R.E. West. *Plant design and economics for engineers, 5th edition*, McGraw Hill, 2004.

[41] M. Pearce, M. Shemfe, and C. Sansom. *Techno-economic analysis of solar integrated hydrothermal liquefaction of microalgae*. Appl. Energy, 2016, 166, 19–26.

[42] C. Beal, L. Gerber, D. Sills et al. "*Algal biofuel production for fuels and feed in a 100-ha facility: A comprehensive techno-economic analysis and life cycle assessment.* Algal Research, 2015, 10, 266–279.

[43] S. Ke Liu. *Hydrogen and Syngas Production and Purification Technologies*. American Institute of Chemical Engineers, 2010.

[44] G. Gahleitner. *Hydrogen from renewable electricity: An international review of power-to-gas pilot plants for stationary applications.* Int. J. Hydrogen Energy, 2013, 38 (5), 2039–2061.

[45] *Water electrolysis & Renewable energy systems.* In: FuelCellToday, 2013.

[46] T. Smolinka. *Water Electrolysis.* In: Encyclopedia of Electrochemical Power Sources, G. Jürgen, Ed. Amsterdam: Elsevier, 2009, pp. 394–413.

[47] B. Yu, W. Zhang, J. Chen, J. Xu, S. Wang. *Advance in highly efficient hydrogen production by high temperature steam electrolysis.* Sci. China Ser. B Chem. , 2008, 51 (4), 289–304.

[48] G. Schiller, A. Ansar, M. Lang, O. Patz. *High temperature water electrolysis using metal supported solid oxide electrolyser cells (SOEC).* J. Appl. Electrochem., 2009, 39 (2), 293–301.

[49] E. Erdle, J. Gross, V. Meyringer. *Possibilities for hydrogen production by combination of a solar thermal central receiver system and high-temperature electrolysis of steam.* In 3rd Intl. workshop on solar thermal central receiver systems, 1986, pp. 727–736.

[50] J. Sigurvinsson, C. Mansilla, P. Lovera, F. Werkoff. *Can high temperature steam electrolysis function with geothermal heat?* Int. J. Hydrogen Energy, 2007, 32 (9), 1174–1182.

[51] E.A. Harvego, M.G. McKellar, J.E. O´Brien, J.S. Herring. *Parametric evaluation of large-scale high-temperature electrolysis hydrogen production using different advanced nuclear reactor heat sources*. Nucl. Eng. Des., 2009, 239, 1571–1580.

[52] J. Sanz-Bermejo, J. Muñoz-Antón, J. Gonzalez-Aguilar, M. Romero. *Optimal Integration of a Solid-Oxide Electrolyser Cell Into a Direct Steam Generation Solar Tower Plant for Zero-Emission Hydrogen Production.* Appl. Energy, 2014, 131, 238–247.

[53] M. Romero, J. González-Aguilar. *Solar thermal power plants: from endangered species to bulk power production in sun-belt regions.* In: Energy and Power Generation Handbook, no. 3, K. R. Rao, Ed. ASME, 2011.

[54] M. Medrano, A. Gil, I. Martorell, X. Potau, and L. F. Cabeza, "*State of the art on high-temperature thermal energy storage for power generation. Part 2 – Case studies*," Renew. Sustain. Energy Rev., vol. 14, no. 1, pp. 56–72, Jan. 2010.

[55] S. Licht, H. Wu. "*STEP iron, a chemistry of iron formation without CO2 emission: molten carbonate solubility and electrochemistry of iron ore impurities*", J. Phys. Chem. C, 2011, 115, 25138–25147.

[56] H. Yin, X. Mao, D. Tang, W. Xiao, L. Xing, H. Zhu, D. Wang, D. Sadoway. *Capture and electrochemical conversion of CO2 to valued-added carbon and oxygen by molten salt electrolysis*. Energy Environ. Sci., 2013, 6, 1538–1545.

[57] C. Graves, S.D. Ebbesen, M. Mogensen, K.S. Lackner. *Sustainable hydrocarbon fuels by recycling CO2 and H2O with renewable or nuclear energy*. Renew. Sust. Energy Rev., 2011, 15, 1–11.

[58] L. Hu, I. Rexed, G. Lindbergh, C. Lagergren, *Electrochemical performance of reversible molten carbonate fuel cells*, Int. J. Hydrogen Energy, 2014, 39 (23), 12323–12329.

[59] T. Wall et al. *An overview on oxyfuel coal combustion – State of the art research and technology development*, Chem. Eng. Res. Des., 2009, 87, 1003-1016.

[60] J.R. Scheffe, A. Steinfeld. *Oxygen exchange materials for solar thermochemical splitting of H2O and CO2: a review*. Materials Today, 2014, 17 (7), 341–348.

[61] P. Furler et al. *Solar thermochemical CO2 splitting utilizing a reticulated porous ceria redox system*. Energy & Fuels, 2012, 26, 7051-7059.

[62] A. H. McDaniel et al. *Nonstoichiometric perovskite oxides for solar thermochemical H2 and CO production*. Energy Procedia, 2014, 49, 2009–2018.

[63] E. Rytter et al. *Process concepts to produce syngas for Fischer–Tropsch fuels by solar thermochemical splitting of water and/or CO2*. Fuel Processing Technology, 2016, 145, 1–8.

[64] M.S. Ferrandon et al. *Hydrogen production by the Cu–Cl thermochemical cycle: Investigation of the key step of hydrolysing CuCl2 to Cu2OCl2 and HCl using a spray reactor*. Int. J. Hydrogen Energy, 2010, 35 (3), 992–1000.